Alignment and Assembly of Graphene Nanoribbons Obtained by Unzipping of Single-Walled Carbon Nanotubes by Dielectrophoresis Method

Alignment and Assembly of Graphene Nanoribbons Obtained by Unzipping of Single-Walled Carbon Nanotubes by Dielectrophoresis Method

by

WAHYU WASKITO AJI

Dissertation submitted in partial fulfilment
of the requirement for the degree of
Doctor of Philosophy

SUPERVISOR:

PROF. HIROFUMI TANAKA

Graduate School of Life Science and Systems Engineering

Kyushu Institute of Technology

2020

TABLE OF CONTENTS

TABLE OF CONTENTS 1

ABSTRACT 4

CHAPTER 1 7

Introduction and Literature Review 7

1.1. General introduction 7

1.2. Carbon Nanotubes 7

1.3. Graphene Nanoribbons 9

1.4. Graphene Nanoribbons Fabrication 11

1.5. Dielectrophoresis 14

1.6. Raman Spectroscopy 18

1.7. Objectives of This Study 20

1.8. Outline of Dissertation 21

1.9. References 21

CHAPTER 2 26

Methodology 26

2.1. Introduction 26

2.2. Chemicals and Materials 26

2.3. Longitudinal Unzipping with Mechanical Sonication 27

2.4. Nanogap Electrode Fabrication 28

2.5. Dielectrophoresis 31

2.6. Atomic Force Microscopy (AFM) 32

2.7. Electrical Characteristics 33

2.8. Raman 33

CHAPTER 3 35

Alignment and Assembly of Graphene Nanoribbons Unzipped Single-Walled Carbon Nanotubes by Dielectrophoresis Method 35

3.1. Abstract 35
3.2. Introduction 35
3.3. Experimental Procedure 37
3.4. Results and Discussion 38
3.4.1. Voltage dependent dielectrophoresis 39
3.4.2. Frequency dependent dielectrophoresis 41
3.4.3. Gap size effect on SWNTs/GNRs dielectrophoresis 43
3.5. Conclusion 45
3.6. Reference 45
CHAPTER 4 49
Frequency Dependence Dielectrophoresis Technique for Graphene Nanoribbons Separations 49
4.1. Abstract 49
4.2. Introduction 49
4.3. Experimental Procedure 51
4.4. Results and Discussion 52
4.5. Conclusion 59
4.6. Reference 60
CHAPTER 5 65
Single Trapping Graphene Nanoribbons Unzipped Single-Walled Carbon Nanotubes by Dielectrophoresis 65
5.1. Abstract 65
5.2. Introduction 65
5.3. Experimental Procedure 66
5.4. Results and Discussion 67
5.5. Conclusion 71
5.6. Reference 71
CHAPTER 6 75

Conclusions and Suggestions 75
LIST OF PUBLICATION 76
LIST OF CONFERENCE 77
ACKNOWLEDEMENT 78

ABSTRACT

Nanoscale electrical devices are one of the biggest challenges for exceeding Moore's law owing to the limitations of fine processing technology in complementary metal-oxide-semiconductors (CMOS). Graphene is one of the most attractive materials due to high carrier mobility and conductivity, which becomes a candidate for replacing CMOS technology. Even though it has superior electrical properties, graphene is zero bandgaps, which means metallic behaving material at finite temparature. Bandgap opening to form semiconductive graphene was necessary for graphene devices application. Various reports suggested producing graphene with sub-10 nm width, called graphene nanoribbons (GNRs), to make the finite bandgap. Several reports showed that sub-10 nm GNRs could be obtained by lengthwise opening or cutting single-walled carbon nanotubes (SWNTs) sidewall or longitudinal unzipping. However, the application of GNR unzipped SWNTs is still limited because of the difficulty of separating the GNRs from excess SWNTs and the assembly process for device fabrication. One possible approach to select sGNRs from CNTs is the dielectrophoresis (DEP) method, which is the nanomaterial alignment method that avoids contamination. DEP is applied in the alignment of nanowires from metal to insulator and in separating materials of differing electrical properties such as metal and semiconductive CNTs (mCNTs and sCNTs, respectively). The separation capability is due to the different DEP forces generated from conductivities and permittivities of utilized materials. These merits indicate that DEP has excellent potential for solving both the separation problem between sGNRs and CNTs and the alignment problem between the electrodes by leveraging different materials' responses to the DEP force.

In this thesis, I reported successfully assembled and separated sGNRs from excess SWNTs using the frequency-dependent dielectrophoresis (DEP) method by varying the

frequency and applied voltage. The peaks from radial breathing mode (RBM) of the Raman spectrum were missing at frequencies higher than 13 MHz. The RBM peaks correlated with SWNTs, suggests that only sGNRs remained after the DEP. The AFM image and RBM Raman peaks also confirm successfully bridged single layer sGNRs by adjusting DEP condition. This result showed that the DEP method can be utilized for alignment and separation of sGNRs obtained from unzipped SWNTs, which is promising for nanocarbon device applications.

The contents of this thesis are the following:

Chapter 1 describes the introduction and literature review covering the theory and literature related to the involved works, research motivation, objectives, and study scope. The literature review includes the introduction of GNRs, fabrication of GNRS, and DEP.

In chapter 2, I describe the materials, chemicals used, and experimental procedures. This chapter includes the experiment's design, the synthesis process of GNRs by longitudinal unzipping, and DEP's experimental set-up. The characterization technique and working principle.

Chapter 3 describes the alignment and assembly of SWNTs/GNRs with the influence of applied voltage, frequency, and gap size of the electrode. The AFM images and presence of D and G band peak in the Raman spectrum confirmed sGNRs with excess SWNTs were successfully bridged by the DEP method. The increase in applied voltage will increase the number of trapped SWNTs/GNRs. The opposite effect was observed in the frequency-dependent DEP, which means that the increase in applied frequency decreased the number of trapped SWNTs/GNRs.

In chapter 4, I describe the separation between sGNRs and mSWNTs with frequency DEP. The metallic SWNTs peaks from radial breathing mode (RBM) were missing at frequencies higher than 13 MHz. The disappear of RBM peak suggests that only sGNRs remained after the DEP. The attractive DEP force of the sGNRs becomes stronger than that of SWNTs under these conditions. This finding was supported by the structural evaluation of bridged SWNTs/sGNRs and the DEP process's theoretical calculations.

In chapter 5, I describe the bridging of single layer sGNRs. By the AFM images and RBM peak, we confirmed the presence of single layer sGNRs trapped via 1 Vpp, 15 MHz, 2μm gap size, and diluted SWNTs/GNRs in 1:50 ratio as DEP condition.

In chapter 6, I conclude that sGNRs are successfully assembled and separated from excess SWNTs via the DEP method.

Keyword: *Dielectrophoresis, graphene nanoribbons, longitudinal unzipping. alignment, separation.*

CHAPTER 1
Introduction and Literature Review

1.1. General introduction

The limitation of silicon technology scaling-down become an obstacle to the development of research and technology. Graphene materials have superior electrical properties compared to silicon over opportunities to replace the technology. Graphene as zero band-gap materials need to reform other carbon-based materials such as graphene nanoribbons for device application. Graphene nanoribbons shows band-gap when the width is less than 10 nm. To produce controllable width of graphene nanoribbons, longitudinal unzipping single-wall carbon nanotubes fabrication process is over high yield and controllable width. Even though promising for large scale fabrication, the application still limited cause by suitable alignment and assemble method and the separation with excess SWNTs. To solve this problem, the dielectrophoresis (DEP) method over the possibility of alignment and separation of GNRs.

This chapter provides background knowledge gathered from literature as guidance on assessing and evaluating the work results. The general properties of carbon nanotubes and graphene nanoribbons, and the theory about longitudinal unzipping, dielectrophoresis, and Raman spectroscopy, will be reviewed here.

1.2. Carbon Nanotubes

Carbon nanotubes are a rolled-up of graphene sheet. It can be a form of single-wall (SWNTs), double-wall (DWNTs), or multi-wall (MWNTs) depend on the number of its concentric cylinder layers. The electrical properties of SWNTs can either metallic or semiconductive depends on the structure specified by two integers (n and m), which

is known as chirality. The type of chirality in SWNTs, as shown in figure 1.1[1], is armchair, zigzag, and chiral[2]. When n-m is multiple of 3, then the nanotubes are metallic or highly conducting nanotubes, and if not, then the nanotubes are semimetallic or semiconductor[3,4].

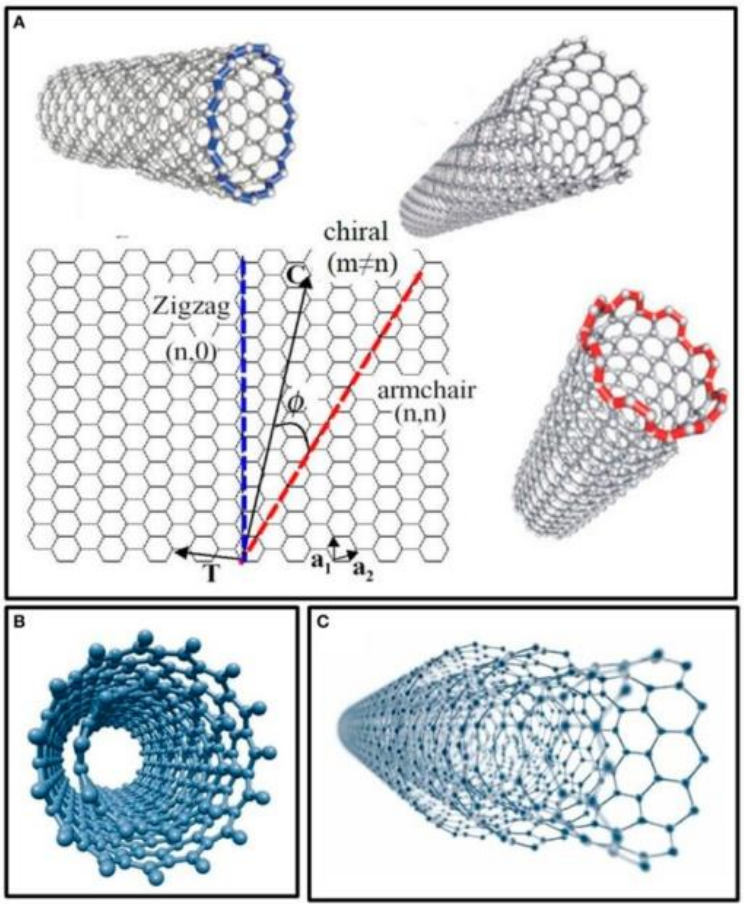

Figure 1.1. Schematic diagram showing zigzag, armchair, and chiral carbon nanotubes (reprint from ref.[1], open-access)

Carbon nanotubes were widely applied in application such as RF transistor[5,6], drug delivery system[7], sensor[8], interconnect[9], and other. Even though it is widely applicable in electronic devices, the greatest challenge in CNT electronic devices is control of the structure properties, i.e. band-gap. To obtain specific chirality of CNTs, chirality-controlled growth and post-growth separation such as gradient-density ultracentrifugation[10], DNA separation[11], gel-column chromatography[12], dielectrophoresis[13], and many more.

1.3. Graphene Nanoribbons

Graphene nanoribbons (GNRs) is a one-dimensional form of graphene. Each GNR could be regarded as finite-width graphene or an unzipped carbon nanotube. The properties of GNRs highly depend on their size and edge shape, which can be zigzag (ZGNR) or armchair (AGNR). Since GNRs are considered periodic across their length, they are usually labeled as N-AGNR and N-ZGNR, where N is the number of carbon atoms along its width, as shown in figure 1.2.

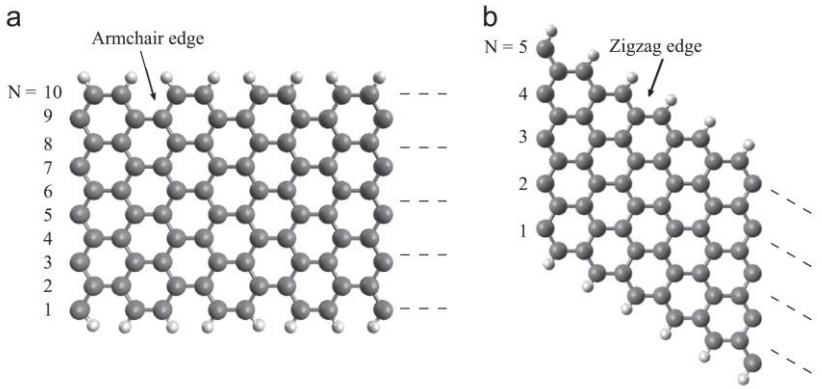

Figure 1.2. The (a) armchair and (b) zigzag edge of GNRs (reprinted from publication ref.[14] with permission from Elsevier)

Depending on the value of ‘‘m’’, the AGNRs can be classified into three categories: m = 3p, 3p + 1, and 3p + 2 (p is a positive integer) with widely varying electronic properties. The periodic AGNRs with m = 3p + 2 shows metallic behavior, whereas the other two show semiconducting behavior within the tight-binding (TB) formalism.

In the other hand, the periodic ZGNRs with the anti-ferromagnetic ground state have been predicted to show a unique property, half-metallicity, while exposed to an external electric field along the cross-ribbon width direction. Unlike conventional metals or semiconductors, half-metallic materials show zero band-gap for electrons with one spin orientation, whereas the other spin channel remains semiconducting or insulating, as

shown schematically in Fig. 1.3[15]. Owing to this unique band property, this class of materials allows only one type of spin to flow under an electric field's influence and thus gives complete control over the spin polarization of current with higher efficiency for magnetic memory storage.

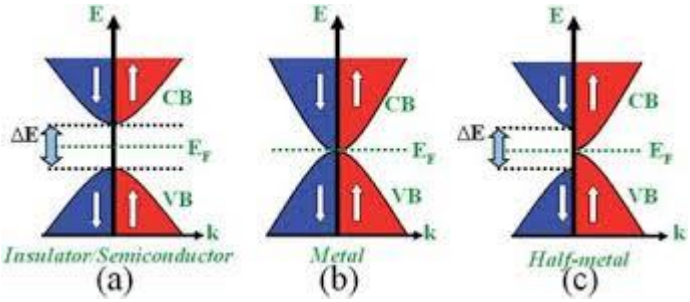

Figure 1.3. Schematic representation of the spin-polarized electronic band structure of (a) insulator or semiconductor, (b) metal, and (c) half-metal (reproduce from ref.[15] with permission from The Royal Society of Chemistry)

Recently, it has been proved experimentally that band-gap in GNRs was influenced by GNRs width. The band-gap as a function of GNR width for six devices was shown in figure 1.4. The band-gap value significantly increased when the GNRs width was less than 20 nm[16,17]. These band-gap properties made GNRs become a suitable candidate for electronic devices application.

Ahmad N. A. and co-worker showed GNRs for chemical sensing applications. The GNRs arrays were fabricated by patterning chemical vapor deposition (CVD) graphene using helium ion beam lithography. The result shows the ability of GNRs FET devices to sensing NO2 gas even in low concentration down to 20 ppb[18]. GNRs transistor for DNA detection also has been done by F. Traversi and co-worker. Solid-state nanopore was integrated with graphene nanoribbons transistor for sensing DNA translocation [19].

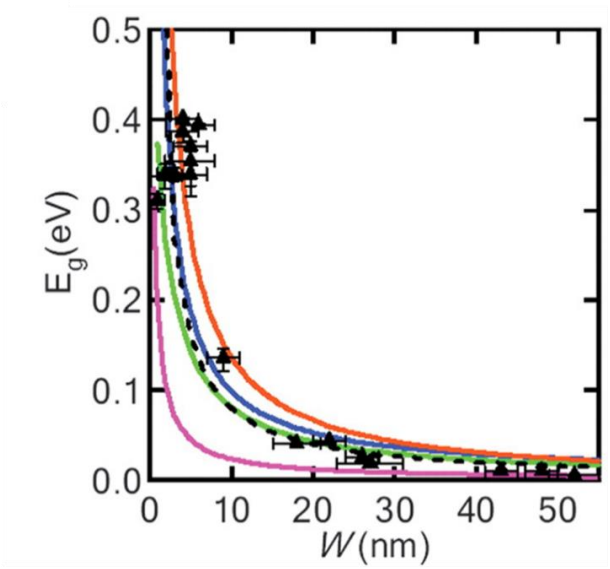

Figure 1.4. Energy gap (E_g) as a function of nanoribbon width, E_g extracted from experimental data (symbols) for various GNRs versus ribbon width. The black dashed line is a fit of our experimental data into an empirical form of E_g (eV) = 0.8/[w(nm)] (from ref [17]. Reprinted with permission from AAAS).

1.4. Graphene Nanoribbons Fabrication

GNRs fabrication method can be separated into a bottom-up and top-down approach, as shown in figure 1.5. Considering the requirement of commercial devices, the research on GNRs fabrication is still extensively conducted to construct technic and devices structure that could make GNRs suitable for commercial use in logic circuit[14].

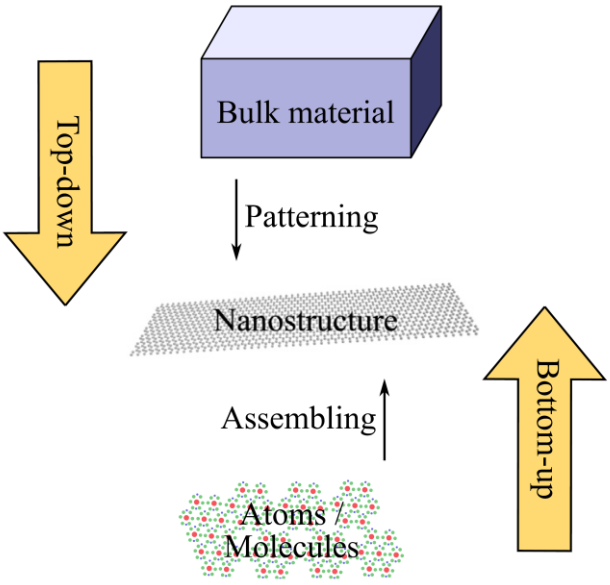

Figure 1.5. Bottom-up and top-down fabrication approach of GNRs (reprinted from publication ref.[14] with permission from Elsevier)

The bottom-up approach was proposed to fabricate GNRs with well-defined and controlled electronic properties. Solution synthesis and on-surface synthesis was an example of a bottom-up approach for GNRs fabrication. J. Cai and co-worker fabricate GNRs using the on-surface synthesis method and successfully produced defect-free AGNRs on Au(111) and Ag (111) surface[20]. Timothy H. Vo and co-worker presented solution-based synthesis method to fabricate GNRs with ~1 nm wide AGNRs with high-aspect-ratio, smooth edges, and band-gap of ~1.3 eV. The produced GNRs length was > 100nm[21].

The Longitudinal unzipping of CNTs was one of top-down approach for GNRs fabrication. Several methods can be used to unzip CNTs, including chemical oxidation, electron beam lithography, plasma etching, mechanical sonication, and others. D. V. Kosynkin and colleagues were successfully cutting and unravelling of MWNTs to form GNRs using the oxidation process. MWNTs was suspending in concentrated sulphuric acid followed by treatment using $KMnO_4$. The proposed method by the author was

shown in figure 1.6. The oxidized edges and defect site made the GNRs have electronic characteristics inferior to the graphene's mechanically peeled sheet.

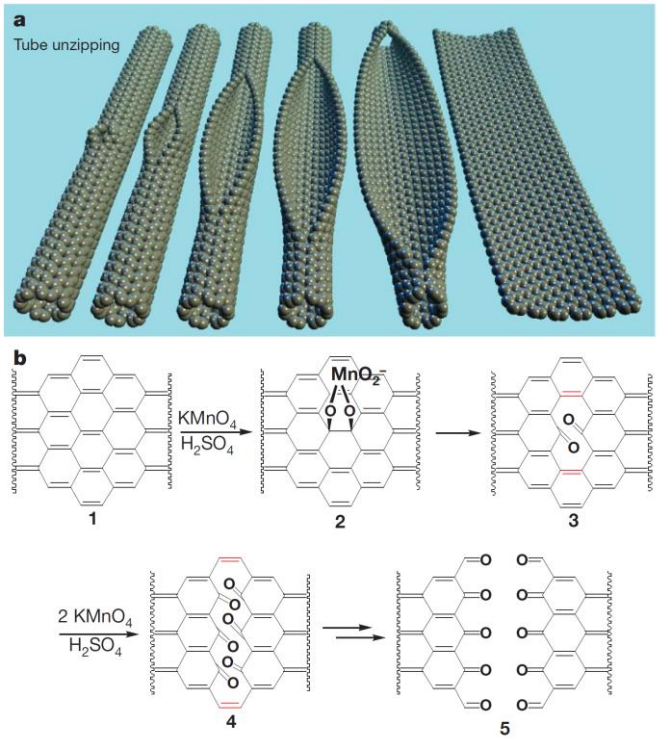

Figure 1.6. Nanoribbon formation and imaging. a. Representation of the gradual unzipping of one wall of a carbon nanotube to form a nanoribbon. Oxygenated sites are not shown. b. The proposed chemical mechanism of nanotube unzipping. The manganate ester in 2 could also be protonated. (reprinted by permission from: Springer Nature ref. [22])

L. Jiao and co-workers obtained high-quality GNRs from mechanical sonication unzipping of MWNTs. The obtained GNRs shown in figure 1.7 have smooth edges, electrical conductance $5e^2/h$, and mobility 1,500 $cm^2\ V^{-1}s^{-1}$ with ribbon width 10-20nm.

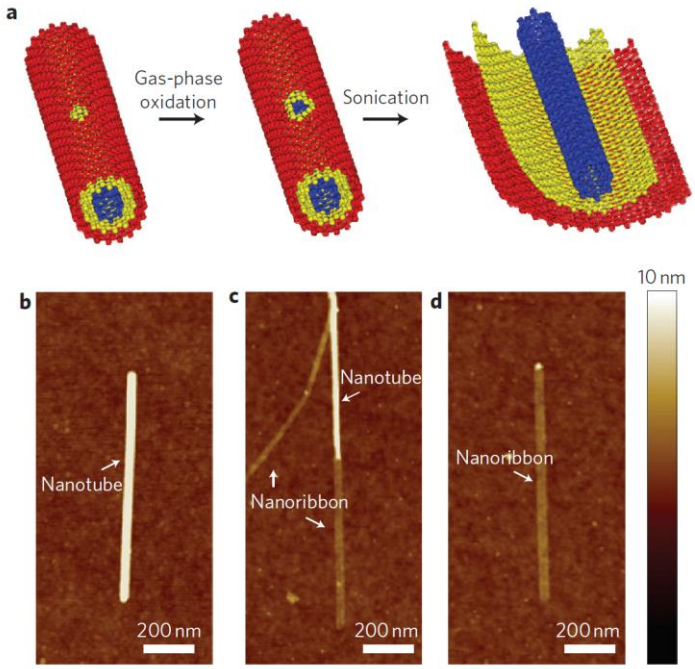

Figure 1.7. Unzipping of nanotubes using a two-step method in gas and liquid phases. a. Schematic of unzipping process, b-d. AFM images of pristine, partially, and fully unzipped (reprinted by permission from: Springer Nature ref. [23]).

1.5. Dielectrophoresis

Dielectrophoresis is the motion of particles due to the interaction of an induced dipole in the particle with a non-uniform electric field. In dielectrophoresis, there are particles and electrolyte. The amount of charge at the interface depends on the field strength and the electrical properties (conductivity and permittivity) of both particles and electrolytes. The field lines for a non-uniform electric field are shown in figures 1.8 (a) and 1.8(b). The particle polarises, and the field lines around the particle behave similarly to the uniform field case. However, by examining the density of electric field lines, we see that the field strength on one side of the particle is greater than the other. This phenomenon leads to an imbalance of forces on the induced dipole, resulting in

particle movement. This effect is called dielectrophoresis. When the particle's polarisability is greater than its surrounding, the direction of the dipole is with the field, and the particle experiences a force called positive DEP; the particle moves towards the strong field region, as shown in figure 1.3(a). The opposite situation gives rise to negative DEP, figure 1.8(b), and the particle moves away from strong electric field regions[24].

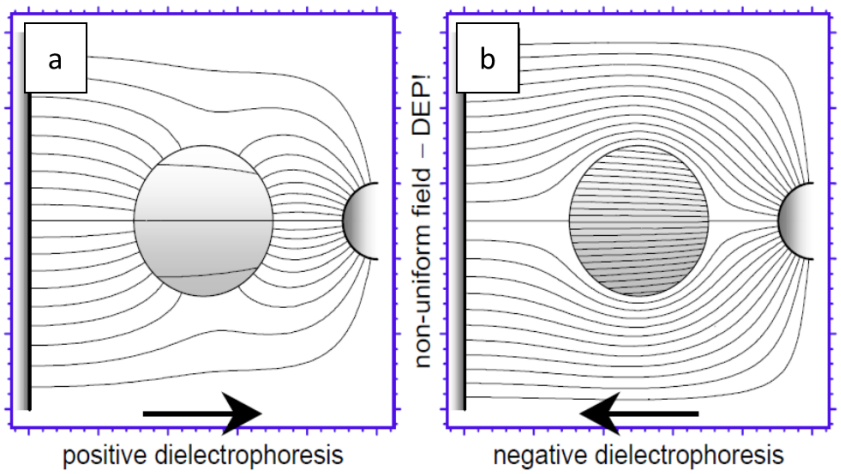

Figure 1.8. Numerically calculated electric field lines for two different cases, defined by the particle more polarizable or less polarizable than the suspending medium, are in a non-uniform electric field. For the more polarizable particle (a) and the less polarizable particle (b). The arrows show the direction of the force and movement in each case (reprinted by permission from: Springer Nature ref.[24])

The force exerted by an electric field **E** on a dipole with dipole moment **p** is given by

$$\mathbf{F} = (\mathbf{p}.\nabla)\mathbf{E}$$

Here the higher-order terms of the force are omitted. Thus, the expression is only accurate if the electric field's magnitude does not vary significantly across the dipole. In an AC field, the time-averaged force on a particle will be given by

$$\boldsymbol{F_{DEP}} = \boldsymbol{\Gamma} \cdot \boldsymbol{\varepsilon_m} \boldsymbol{Re\{CM\}} \boldsymbol{\nabla E}$$

where **Γ** is a factor depending on geometry, εm is the real part of the suspending medium's permittivity and **E** is the electric field. The factor CM depends on the

complex permittivities of both the particle and the medium. In the case of a spherical particle, this factor is referred to as the Clausius–Mossotti Factor. In the particle object, the CM is given by

$$\boldsymbol{CM} = \frac{\boldsymbol{\varepsilon_p}^* - \boldsymbol{\varepsilon_m}^*}{\boldsymbol{\varepsilon_p}^* + \boldsymbol{2\varepsilon_m}^*}, \qquad \boldsymbol{\varepsilon}^* = \boldsymbol{\varepsilon} - \boldsymbol{i}\frac{\boldsymbol{\sigma}}{\boldsymbol{\omega}}$$

but for an elongated object with the long axis aligned with the field, CM is given by

$$\boldsymbol{CM} = \frac{\boldsymbol{\varepsilon_p}^* - \boldsymbol{\varepsilon_m}^*}{\boldsymbol{\varepsilon_m}^*}, \qquad \boldsymbol{\varepsilon}^* = \boldsymbol{\varepsilon} - \boldsymbol{i}\frac{\boldsymbol{\sigma}}{\boldsymbol{\omega}} \ ,$$

where the indices p and m refer to the particle and the medium, respectively. Here σ is the conductivity, ε the real permittivity, and $\omega = 2\pi f$ the angular frequency of the applied electric field[25,26].

In the case of the elongated object with the long axis aligned with the field such as CNT, the $\boldsymbol{\Gamma}$ can be written as

$$\boldsymbol{\Gamma} = \frac{\boldsymbol{1}}{\boldsymbol{6}}\boldsymbol{\pi r^2 l}$$

where r is the radius and l the length of CNT[25,27].

Dielectrophoresis was widely used on trapping and separation of material such as cancer cell[28], DNA and blood[29], nanowire[30], and also CNT[31,32]. Krupke R. and co-worker were separate metallic from semiconducting SWNTs using dielectrophoresis. Metallic SWNTs were trapped on the electrode, and semiconducting SWNTs were left in the solvent. A dark-field micrograph was used to analyze the trapped SWNTs. Strong Rayleigh scattered light made trapped SWNTs appear in green color, as shown in figure 1.9. The separation of SWNTs was achieved up to 80% of the enrichment of metallic tubes.

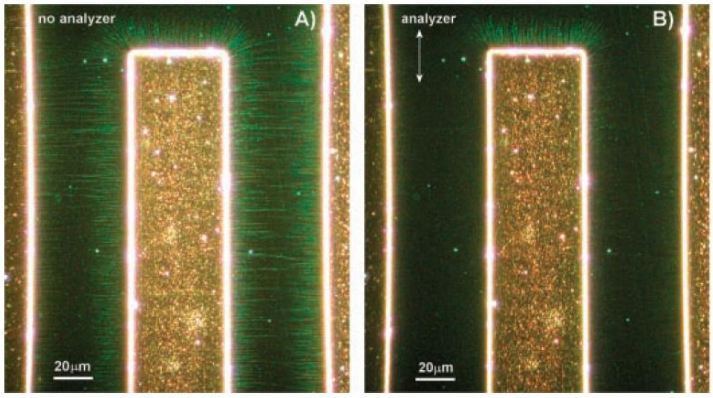

Figure 1.9. Rayleigh scattered light from the dielectrophoretically deposited SWNTs and the electrodes, recorded with an incident-light dark-field microscope. The scattered light from the aligned SWNTs appears green to the eye (**A**) and is polarized perpendicular to the electrodes (**B**) (reprinted by permission from: Springer Nature ref. [33]).

Maria D. and Peter B. are using a numerical study to calculate the probability of capturing metallic and semiconductor SWNTs using dielectrophoresis. The result suggests relatively low frequencies when both metallic and semiconducting SWNTs were optimal for the separation process due to large differences in dielectric force[25]. Freer and co-worker were successfully aligned single gold nanowire with high precision and yield using dielectrophoresis, as shown in figure 1.10. At low voltages, the dielectric force is insufficient to trap a nanowire on an electrode. As the dielectrophoretic forces overcome fluid drag forces, nanowires become trapped on the electrodes. Only single nanowires assemble over an extensive voltage range (20% of the applied voltage). Lines are interpolated in the transition regime.

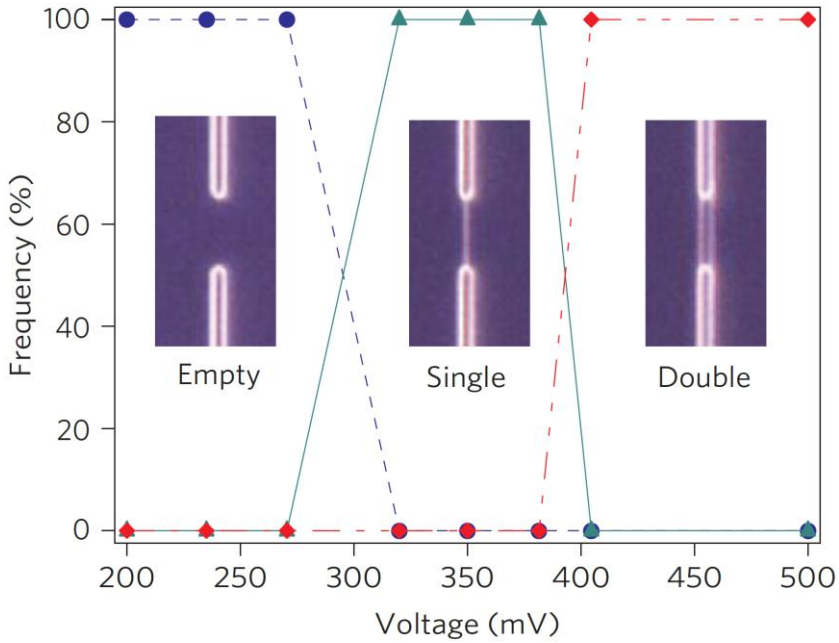

Figure 1.10. Critical pinning voltages for nanowire assembly. The event frequency is shown for empty electrodes (blue circles), a single nanowire (green triangles), and double nanowires (red diamonds) for a total of 50 sites. Frequency and flow rates are 500 Hz and 1.3 ml min21, respectively. Electrode dimensions: 12 mm gap, 2mm width (reprinted by permission from: Springer Nature ref. [30]).

Single gold nanowire trapping process was adjusted by controlling applied voltage, and flow rate of fluid contain gold nanowire (dielectrophoresis and hydrodynamic forces)[30].

1.6. Raman Spectroscopy

In the Raman spectra of graphite and SWNTs, many features can be identified specific phonon modes and with specific Raman scattering processes that contribute to each part. The Raman spectra of graphite and SWNTs can provide us with much information about the exceptional 1D properties of carbon materials, such as their phonon structure and their electronic structure, and information about sample imperfections (defects). Since mechanical properties, elastic properties, and thermal

properties are strongly influenced by phonons, Raman spectra provide much general information about the structure and properties of SWNTs[34].

Raman scattering is the inelastic scattering of light. During a scattering event:

1. An electron is excited from the valence energy band to the conduction energy band by absorbing a photon.
2. Emitting (or absorbing) phonons scatter the excited electron.
3. The electron relaxes to the valence band by emitting a photon.

We generally observe Raman spectra for the scattered photon (light) whose energy is smaller by the phonon energy than the incident photon. By measuring the intensity of the scattered light as a function of frequency downshift (losing energy) of the scattered light, which is plotted in Raman spectra, we obtain an accurate measure of the material's phonon frequencies. By combining this information with the original geometrical structure of a crystal (or molecule), we can deduce a model for the phonon dispersion relations (or normal mode frequencies)[34]

The number of emitted phonons before the relaxation of the lattice can be one, two, and so on, which we call, respectively, one-phonon, two-phonon, and multi-phonon Raman processes. The order of a scattering event is defined as its number in the sequence of the total scattering events, including elastic scattering by an imperfection (such as a defect or edge) of the crystal. The lowest order process is the first-order Raman scattering process, which gives Raman spectra involving one-phonon emission, as shown in figure 1.11. A scattering event with only elastic scattering, i.e., photon direction change but no frequency shift, corresponds to Rayleigh scattering of light. In SWNTs, the G band spectra, which is split into many features around 1580 cm^{-1}, and the lower frequency radial breathing mode (RBM) is usually the strongest features in SWNT Raman spectra are both first-order Raman modes. The RBM is a unique phonon

mode, appearing only in carbon nanotubes and its observation in the Raman spectrum provides direct evidence that a sample contains SWNTs. The RBM is a bond-stretching out-of-plane phonon mode for which all the carbon atoms move coherently in the radial direction, and whose frequency ω_{RBM} is about 100–500 cm^{-1}. The RBM frequency is inversely proportional to the tube diameter and is expressed as $\omega_{RBM} = C/d_t$ (cm^{-1}).

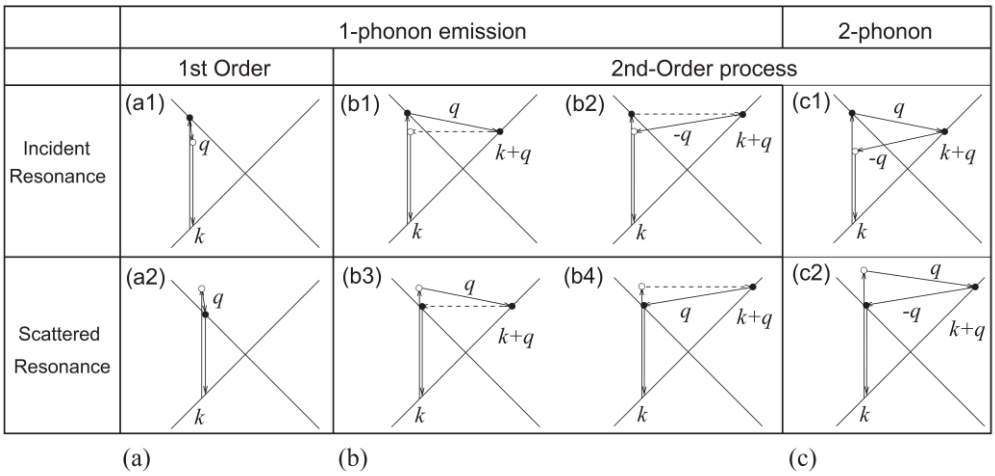

Figure 1.11. (a) First-order and (b) one-phonon second-order, (c) two-phonon second-order, resonance Raman spectral processes (top) incident photon resonance and (bottom) scattered photon resonance conditions. For one-phonon, second-order transitions, one of the two scattering events is an elastic scattering event (dashed lines). Resonance points are shown as solid circles (reprint from ref. [34] with permission from Elsevier).

Resonance Raman spectra from SWNTs can be acquired using standard commercial micro-Raman spectrometers and lasers. Typical measurements use a back-scattering configuration and ×50, ×80, and ×100 objective lenses (~ 1 m spot size for the 100× objectives). Relatively high laser powers (up to 40×10^9 W m^{-2}) can probe isolated SWNTs on substrates or in aqueous solution because of their unusually high thermal conductivity values (3000 W mK^{-1})[34].

1.7. Objectives of This Study

The main objects of the research are:

a. To align and assemble graphene nanoribbons (GNRs) fabricated by longitudinal unzipping single-walled carbon nanotubes (SWNTs) using the dielectrophoresis technique.
b. To separate graphene nanoribbons (GNRs) with excess single-walled carbon nanotubes (SWNTs) using the dielectrophoresis technique.
c. To produce a single layer alignment of graphene nanoribbons (GNRs) using the dielectrophoresis technique.

1.8. Outline of Dissertation

This dissertation consisted of 6 chapters. Chapter one explains the introduction and literature review covering the theory and literature related to these work's work, objectives, and study scope. Chapter two describes the material and chemical used in this work, the experimental procedures, and the apparatus used to characterize it.

Chapter three, four and five focus on presenting result and analysis of experiment in the form of journal template. The chapter is organized to abstract, introductory, experimental procedures, results, and discussions, conclusions. Chapter six states the overall findings of this work as well as some suggestions and recommendations.

1.9. References

1. Tilmaciu, C. M. & Morris, M. C. Carbon Nanotubes Biosensor. *Front. Chem.* **3**, 59 (2015)
2. Rahmandoust, M. & Öchsner, A. Buckling behaviour and natural frequency of zigzag and armchair single-walled carbon nanotubes. *J. Nano Res.* **16**, 153–160 (2012).
3. Eatemadi, A., Daraee, H., Karimkhanloo, H., Kouhi, M., Zarghami, N., Akbarzadeh, A., Abasi, M., Hanifehpour, Y. & Joo, Sang W. Carbon nanotubes:

Properties, synthesis, purification, and medical applications. *Nanoscale Res. Lett.* **9**, 1–13 (2014).

4. Saito, R., Nugraha, A. R. T., Hasdeo, E. H., Hung, N. T. & Izumida, W. Electronic and Optical Properties of Single Wall Carbon Nanotubes. *Top. Curr. Chem.* **375**, 1–24 (2017).

5. Zhong, D., Shi, H., Ding, L., Zhao, C., Liu, J., Zhou, J., Zhang, Z. & Peng, L. M. Carbon Nanotube Film-Based Radio Frequency Transistors with Maximum Oscillation Frequency above 100 GHz. *ACS Appl. Mater. Interfaces* **11**, 42496–42503 (2019).

6. Lan, Y., Yang, Y., Wang, Y., Wu, Y., Cao, Z., Huo, S., Jiang, L., Guo, Y., Wu, Y., Yan, B., Xu, R., Chen, Y., Chen, Y., Li, Y., Lal, S., Ma, Z. & Xu, Y. High-Temperature-Annealed Flexible Carbon Nanotube Network Transistors for High-Frequency Wearable Wireless Electronics. *ACS Appl. Mater. Interfaces* **12**, 26145–26152 (2020).

7. Chen, Z., Pierre, D., He, H., Tan, S., Pham-huy, C., Hong, H. & Huang, J. Adsorption behavior of epirubicin hydrochloride on carboxylated carbon nanotubes. *Int. J. Pharm.* **405**, 153–161 (2011).

8. Chopra, S., McGuire, K., Gothard, N., Rao, A. M. & Pham, A. Selective gas detection using a carbon nanotube sensor. *Appl. Phys. Lett.* **83**, 2280–2282 (2003).

9. Sekitani, T., Noguchi, Y., Hata, K., Fukushima, T., Aida, T. & Someya, T. A rubberlike stretchable active matrix using elastic conductors. *Science.* **321**, 1468–1472 (2008).

10. Arnold, M. S., Green, A. A., Hulvat, J. F., Stupp, S. I. & Hersam, M. C. Sorting carbon nanotubes by electronic structure using density differentiation. *Nat.*

Nanotechnol. **1**, 60–65 (2006).

11. Ao, G., Streit, J. K., Fagan, J. A. & Zheng, M. Differentiating Left- and Right-Handed Carbon Nanotubes by DNA. *J. Am. Chem. Soc.* **138**, 16677–16685 (2016).
12. Tanaka, T., Jin, H., Miyata, Y. & Kataura, H. High-yield separation of metallic and semiconducting single-wall carbon nanotubes by agarose gel electrophoresis. *Appl. Phys. Express* **1**, 1140011–1140013 (2008).
13. Krupke, R., Hennrich, F., Löhneysen, H. v. & Kappes, M. M. Separation of Metallic from Semiconducting Single-Walled Carbon Nanotubes. *Science* **301** (5631), 344-347 (2003).
14. Marmolejo-tejada, J. M. & Velasco-medina, J. Review on graphene nanoribbon devices for logic applications. *Microelectronics J.* **48**, 18–38 (2016).
15. Dutta, S. & Pati, S. K. Novel properties of graphene nanoribbons: A review. *J. Mater. Chem.* **20**, 8207–8223 (2010).
16. Han, M. Y., Özyilmaz, B., Zhang, Y. & Kim, P. Energy band-gap engineering of graphene nanoribbons. *Phys. Rev. Lett.* **98**, 206805 (2007).
17. Li, X., Wang, X., Zhang, L., Lee, S. & Dai, H. Chemically Derived, Ultrasmooth Graphene Nanoribbon Semiconductors. *Science* **319**, 1229-1232 (2008).
18. Abbas, A. N., Liu, G., Liu, B., Zhang, L., Liu, H., Ohlberg, D., Wu, W. & Zhou, C. Chemical Sensing Applications of Graphene Nanoribbon Arrays Down to 5 nm Using Helium Ion Beam. 1538–1546 (2014).
19. Traversi, F., Raillon, C., Benameur, S. M., Liu, K., Khlybov, S., Tosun, M., Krasnozhon, D., Kis, A. & Radenovic, A. Detecting the Translocation of DNA Through a Nanopore Using Graphene Nanoribbons. *Nat. Nanotechnol.* **8**, 939–945 (2013).

20. Cai, J., Ruffieux, P., Jaafar, R., Bieri, M., Braun, T., Blankenburg, S., Fasel, R., Muoth, M., Seitsonen, A. P., Saleh, M., Feng, X. & Mu, K. Atomically precise bottom-up fabrication of graphene nanoribbons. **466**, 470–473 (2010).

21. Vo, T. H., Shekhirev, M., Kunkel, D. A. Morton, M. D., Berglund, E., Kong, L., Wilson, P. M., Dowben, P. A., Enders, A. & Sinitskii, A. Large-scale solution synthesis of narrow graphene nanoribbons. *Nat. Commun.* 1–8 (2014).

22. Kosynkin, D. V., Higginbotham, A. L., Sinitskii, A., Lomeda, J. R., Dimiev, A., Price, B. K. & Tour, J. M. Longitudinal unzipping of carbon nanotubes to form graphene nanoribbons. *Nature* **458**, 872–876 (2009).

23. Jiao, L., Wang, X., Diankov, G., Wang, H. & Dai, H. Facile synthesis of high-quality graphene nanoribbons. *Nat. Nanotechnol.* **5**, 321–325 (2010).

24. Morgan, H. & Green, N. G. *AC Electrokinetics*. *Encyclopedia of Nanotechnology* (2012). doi:10.1007/978-90-481-9751-4_100005.

25. Dimaki, M. & Bøggild, P. Dielectrophoresis of carbon nanotubes using microelectrodes: A numerical study. *Nanotechnology* **15**, 1095–1102 (2004).

26. Morgan, H. & Green, N. G. Dielectrophoretic manipulation of rod-shaped viral particles. *J. Electrostat.* **42**, 279–293 (1997).

27. Kim, J. E. & Han, C. S. Use of dielectrophoresis in the fabrication of an atomic force microscope tip with a carbon nanotube: A numerical analysis. *Nanotechnology* **16**, 2245–2250 (2005).

28. Zahedi Siani, O., Zabetian Targhi, M., Sojoodi, M. & Movahedin, M. Dielectrophoretic separation of monocytes from cancer cells in a microfluidic chip using electrode pitch optimization. *Bioprocess Biosyst. Eng.* **43**, 1573–1586 (2020).

29. Sonnenberg, A., Marciniak, J. Y., Krishnan, R. & Heller, M. J. Dielectrophoretic

isolation of DNA and nanoparticles from blood. *Electrophoresis* **33**, 2482–2490 (2012).

30. Freer, E. M., Grachev, O., Duan, X., Martin, S. & Stumbo, D. P. High-yield self-limiting single-nanowire assembly with dielectrophoresis. *Nat. Nanotechnol.* **5**, 525–530 (2010).

31. Le Louarn, A., Kapche, F., Bethoux, J. M., Happy, H., Dambrine, G.,Derycke, V., Chenevier, P., Izard, N., Goffman, M. F. & Bourgoin, J. P. Intrinsic current gain cutoff frequency of 30 GHz with carbon nanotube transistors. *Appl. Phys. Lett.* **90**, 3–6 (2007).

32. Rabbani, M. T., Schmidt, C. F. & Ros, A. Single-Walled Carbon Nanotubes Probed with Insulator-Based Dielectrophoresis. *Anal. Chem.* **89**, 13235–13244 (2017).

33. Marquardt, C. W., Grunder, Sergio., Alfred B., Dehm, S., Hennrich, F., Lo¨hneysen, H. v., Mayor, M. & Krupke, R. Electroluminescence from a single nanotube-molecule-nanotube junction. *Nat. Nanotechnol.* **5**, 863–867 (2010).

34. Dresselhaus, M. S., Dresselhaus, G., Saito, R. & Jorio, A. Raman spectroscopy of carbon nanotubes. **409**, 47–99 (2005).

CHAPTER 2
Methodology

2.1. Introduction

This chapter is divided into three main parts:

1. Materials and chemicals used
2. The process for sample synthesis
3. The characterizations of the fabricated sample including atomic force microscopy imaging, Raman spectroscopy, and electrical properties

2.2. Chemicals and Materials

The materials and chemical used in this research are presented in Table 2.1

Table 2.1. Summary of chemicals and materials used

Chemical Name	Chemical Formula	Function	Supplier	Remarks
Single-Walled Carbon Nanotubes		Unzipping Material	Nanointegris	Purified HipCo
Poly[(*m*-phenylenevinylene)-*co*-(2,5-dioctoxy-*p*-phenylenevinylene)] (PmPV)	$C_{32}H_{46}O_2$	Radical Initiator	Sigma Aldrich	Colour: Yellow Form: Powder
1,2-Dichloroethane	C_2H_4Cl	Solvent	Wako	Purity: 98.0% MW: 98.96 g/mol
Chloroform	$CHCl_3$	Cleansing Agent	Wako	Purity:99.0%

				MW: 119.38 g/mol
Hydrochloric Acid	HCl	Solvent	Wako	Concentration: 36% MW: 36.46 g/mol
Acetone	$(CH_3)_2CO$	Cleansing Agent	Wako	Purity:99.0% MW:58.08 g/mol
Ethanol	C_2H_6O	Solvent	Wako	Purity: 99.5% MW: 46.07 g/mol
Isopropanol	$(CH_3)_2CHOH$	Cleansing Agent	Kanto Chemical	Purity: 99.9% MW: 60.10 g/mol
ZEP-520		Electron Beam Resist		
Anisole	C_7H_8O	Electron Beam Resist	Kanto Chemical	Purity: 89% MW: 108.14 g/mol
n-Amyl Acetate (ZED N-50)	$C_7H_{14}O_2$	Developing Agent	Zeon Chemical	Purity: 100% MW: 130.19 g/mol
Dymethil Sulfoxide	$(CH_3)_2SO$	Lift-off Solution	Kanto Chemical	Purity: 99% MW: 78.14%

2.3. Longitudinal Unzipping with Mechanical Sonication

HipCo SWNTs (Nanointegris) was annealed at 200℃ for 20 hours to remove amorphous carbon, and then acid-treated with HCl with 11.65 M at 109℃ to remove catalyst metal and to induced defects. The GNRs were synthesized by unzipping 0.01

mg of SWNTs (HipCo Purified: Nanointegris) using 3 mg poly [(m-phenylenevinylene)-co-(2,5-dioctoxy-p-phenylene-vinylene)] (PmPV; Sigma-Aldrich) in 10 mL dichloroethane solvent. The solution was bath sonicated for 50 minutes at 37 kHz and 600 W (SHARP UT-606) to initiate the unzipping process.

After sonication, the solution was centrifuged for 16 hours at 50,000 G (TOMY Suprema 23 High-Speed Centrifuge) to reduce the remaining SWNTs. Afterward, the remaining solution (supernatant) was diluted with dichloroethane to reduce the concentration of mixture SWNTs/GNRs in solutions. The overall process was illustrated in figure 2.1.

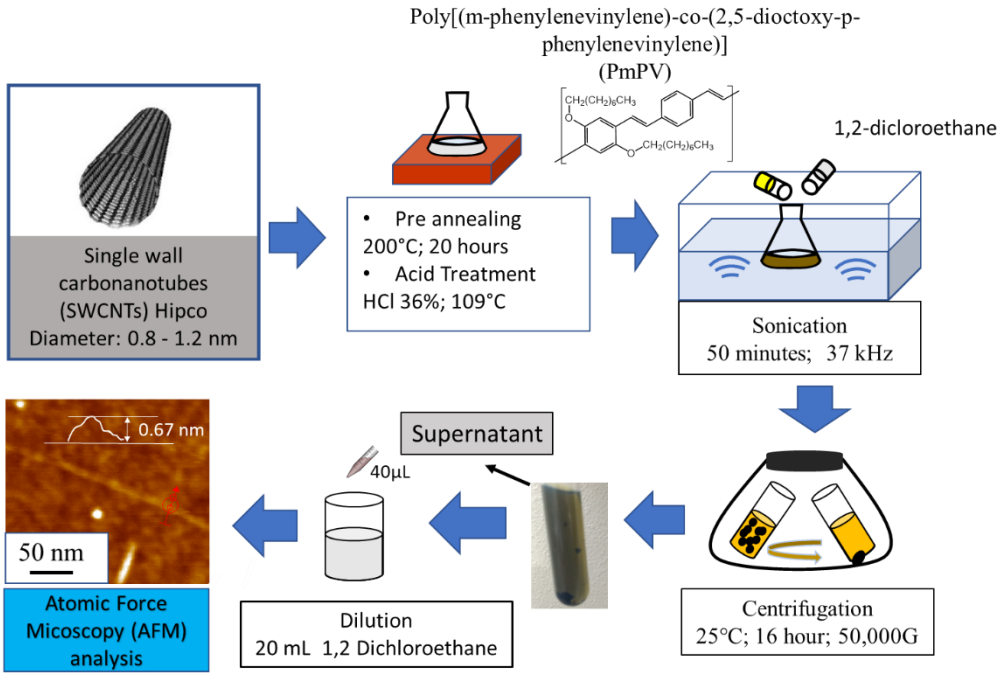

Figure 2.1. Schematic illustration of longitudinal unzipping with mechanical sonication

2.4. Nanogap Electrode Fabrication

A nanoscale gap electrode was fabricated via the EB lithography method, with SiO_2 as the substrate. Firstly, the device pattern was designed by the software

Layout Editor before the process. After that, EB resists solution (gL 2000:anisole = 1:1) was spin-coated to the substrate with speed 5000 rpm for 40 s and pre-baked at 180 ℃ for 3 min. The electrode patterning was performed by the EB machine model Elionix ELS-7500, as shown in Figure 2.2. The beam amplitude was 30 nA and developed by ZED-N 50 solution for 2.5 min continued by MIBK:IPA for 15 sec, then rinsed by distilled water. The material of the electrode was Pt/Ti with a thickness 24/6 nm that depositing by sputtering machine model Miller CFS-4EP-LL, as shown in figure 2.3. The resist then was removed by dimethyl-sulfoxide at 80 ℃ for 40 min under the sonication process. The overall EBL process is illustrated in Figure 2.4.

Figure 2.2. EB-lithography system model Elionix ELS-7500

Figure 2.3. Sputtering machine model Miller CFS-4EP-LL

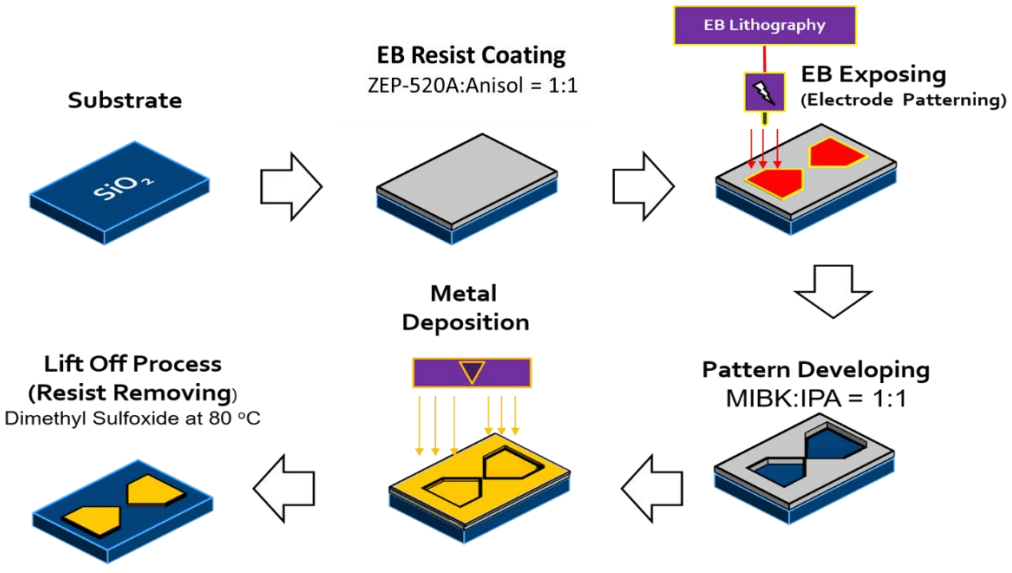

Figure 2.4. Schematic illustration of nanogap electrode fabrication by EBL

The fabricated electrode was investigated using AFM to know the gap condition of the electrode. The AFM of the fabricated electrode with a 2 µm gap was shown in figure 2.5.

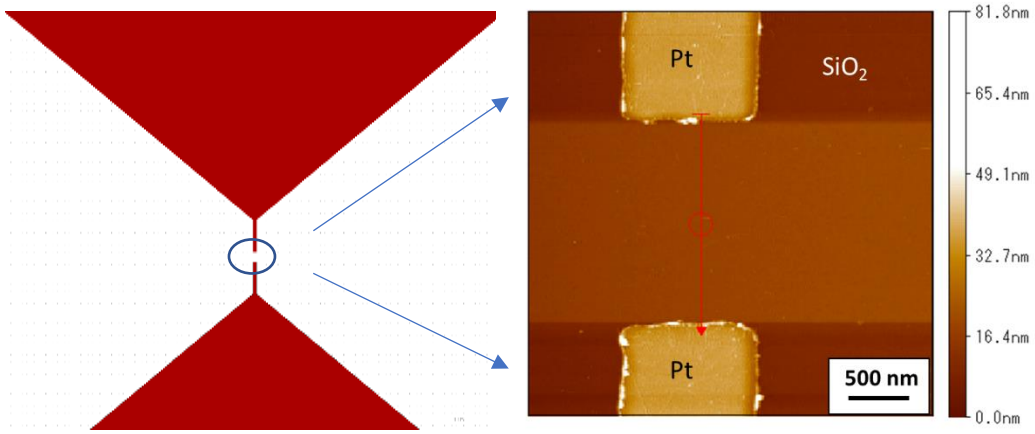

Figure 2.5 Fabricated Electrode with 2µm gap size

2.5. Dielectrophoresis

The AC applied voltage was connected to the sample Pt/Ti electrode by a 50Ω coaxial probe. The solution of SWNTs/GNRs obtained above was cast around the gap of Pt/Ti electrodes, followed by the DEP process. The casted solution was waited for drying around 2 min. This process was repeated for several different DEP parameters such as frequencies, ranging from 500 kHz to 15 MHz and applied voltage ranging from 1 to 10 V using a function generator (33120A Hewlett Packard). The DEP process was illustrated in figure 2.5.

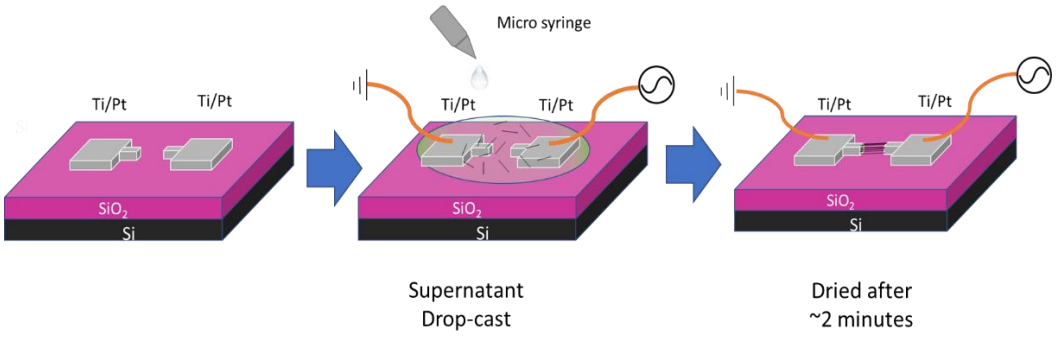

Figure 2.5. Schematic of DEP procedures

After the DEP process, the sample was cleaned with chloroform, dichloroethane, acetone, ethanol, DI water, and subsequently annealed at 200 ℃ for 1.5 hours to remove PmPV, dust and to increase the adhesion between GNRs and electrodes.

2.6. Atomic Force Microscopy (AFM)

After the cleaning process, the DEP sample was investigated with atomic force microscopy (AFM) system model Jeol SPM-5200, as shown in figure 2.6. The scanning process was conducted in ambient condition-tapping mode. Most of the GNR observed with a height of approximately 0.6 nm and a length of 1 to 2 um. The image's quality depends on the cantilever tip and the operator's skill to control the software for adjusting proper laser alignment. The slow scanning rate and scan size also become a parameter of image quality.

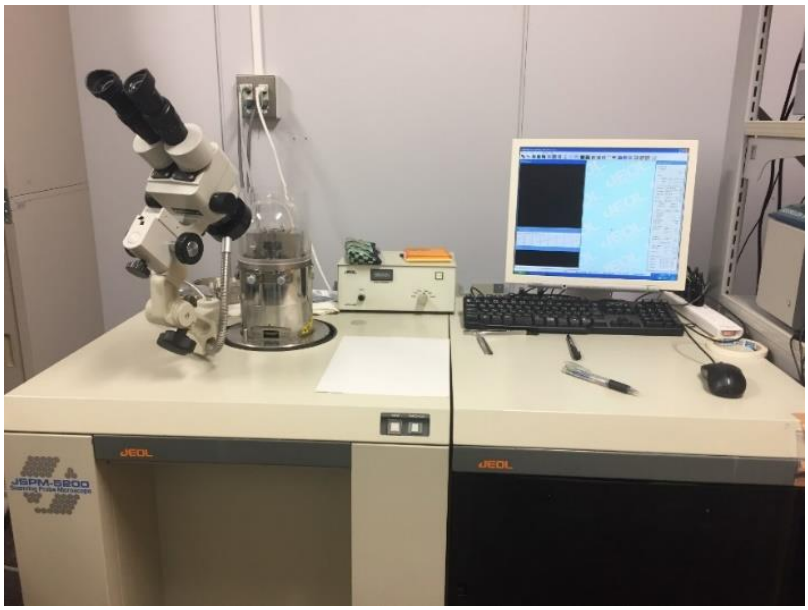

Figure 2.6. AFM system Jeol-SPM 5200

2.7. Electrical Characteristics

The electrical characteristic of samples was investigated by a tailor-made probing system, equipped with a cryogenic freezer, to conduct an *I-V* measurement at low temperature. The photograph of the machine is displayed in Figure 2.7. The current-voltage data were recorded using Keysight Agilent 4156 A semiconductor parameter analyzer. The measurement was conducted in ambient and vacuum condition.

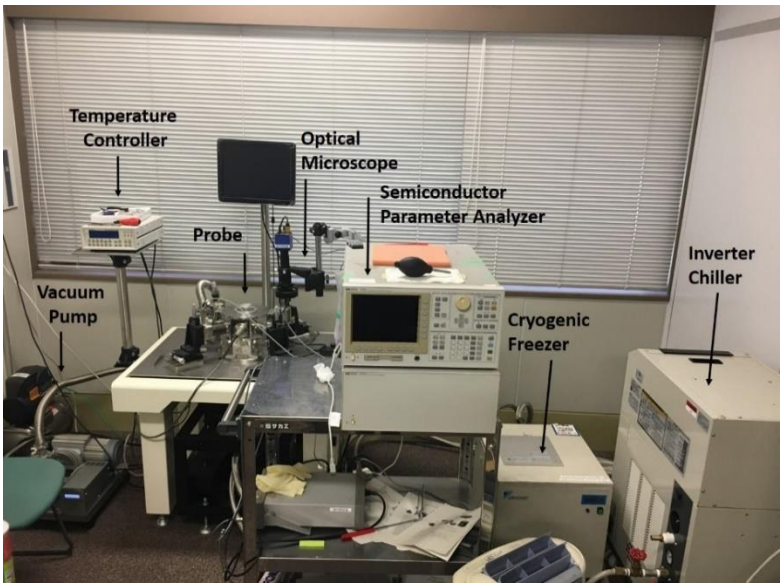

Figure 2.7. Photograph of a probing system equipped with cryogenic freezer

2.8. Raman

The DEP sample was measured using Raman microscopy Nano Photone model Raman Touch as displayed in figure 2.8. The sample was irradiated with 532 nm laser, and the laser excitation power was adjusted from 0.2 mW to 13 mW depend on the sample conditions. The grating-step of each interval data used in this measurement is 600 gr/mm and 2400 gr/mm with 2 s exposure time.

Figure 2.8. Raman microscopy Raman Photonic model Raman Touch

CHAPTER 3
Alignment and Assembly of Graphene Nanoribbons Unzipped Single-Walled Carbon Nanotubes by Dielectrophoresis Method

3.1. Abstract

Graphene nanoribbons (GNRs) fabrication with longitudinal unzipping of carbon nanotubes (CNTs) by mechanical sonication was attractive, causing high yield, smooth edges, and controllable width devices application caused by alignment and assembly problem. Here, we report successfully aligned and trapped GNRs from longitudinal unzip with the dielectrophoresis (DEP) method. The number of trapped SWNTs/GNRs can be adjusted by varying applied voltage and frequency DEP. Increasing applied voltage will increase the number of trapped SWNTs/GNRs while the opposite effect on frequency. The electrode's gap size will influence the alignment form of SWNTs/GNRs, where similar gap size with GNRs length can produce direct alignment without folding and double connection. This result shows the capability of control GNRs alignment and trapping process with the DEP method, which suitable for future devices applications.

3.2. Introduction

The development of science and technology comes with a trend of smaller and smarter electronic devices that increase the need for the number of transistors in each device to follow Moore's law scale. Nanoscale electrical wiring is one of the biggest challenges for exceeding Moore's law owing to the limitations of fine processing technology in CMOS[33,35–37]. Graphene nanoribbons (GNRs), which are stripe-shaped single-atomic layer graphite, have been widely investigated due to their high electronic

mobility, strong mechanical endurance, and high flexibility[38,39]. The electrical properties of GNRs are strongly dependent on the width[16]. When GNRs is more than 10 nm in width, they exhibit semimetallic behavior.

On the other hand, when GNRs are less than 10 nm in width, they exhibit semiconductive behavior because their conduction mechanism becomes quasi-one-dimensional, resulting in an opening in their band-gap. Although several approaches to obtain GNRs, longitudinal unzipping of carbon nanotubes (CNTs) is one of the most common techniques to get semiconductor GNRs measuring a few nanometers in width (sGNRs) [16,40]. In our previous work, we successfully obtained single-layer sGNRs from single-walled[41,42] and double-walled[43–45] carbon nanotubes (SWNTs and DWNTs, respectively) by the unzipping method incorporating an ultrasonication process. Although sub-10 nm width sGNRs can be produced by the unzipping method and is suitable for mass production[22], its application in electronic devices is still limited because of alignment and assemble problem.

One possible approach for aligning and assembly GNRs in the dielectrophoresis (DEP) technique[46–48], which is the method for nanomaterial alignment without any contamination. It is applied both in the alignment of nanowires from metal to insulate and in separating different electrical properties such as metal and semiconductor CNTs (mCNTs and sCNTs, respectively). The separation capability is owed to the various DEP forces generated from different conductivity and permittivity in each material[25,30,47,49,50]. These merits indicate that DEP has excellent potential for solving both the separation problem between sGNRs and CNTs and the alignment problem between the electrodes by leveraging the DEP force's different responses.

Here, we fabricated sGNRs from SWNTs using the unzipping method and assemble

and align it by the DEP process.

3.3. Experimental Procedure

HipCo SWNTs (Nanointegris) were annealed at 200 °C for 20 h to remove amorphous carbon and then acid-treated with HCl (11.65 M at 109 °C) to remove the catalyst metal and induce defects. The GNRs were synthesized by unzipping 0.01 mg of SWNTs using 3 mg poly [(m-phenylenevinylene)-co-(2,5-directory-p-phenylene-vinylene)] (PmPV; Sigma-Aldrich) in 10 mL dichloroethane solvent. The solution was bath sonicated for 50 min at 37 kHz and 600 W (SHARP UT-606) to initiate the unzipping process. The solution was then centrifuged for 16 h at 50,000 G (TOMY Suprema 23 High-Speed Centrifuge) to reduce the remaining SWNTs. The remaining solution (supernatant) was diluted with dichloroethane to reduce the concentration of the mixture SWNTs/GNRs in solution.

Micro-gap electrodes for DEP were fabricated by electron-beam lithography (EBL) on a SiO2 substrate. The residue solution (ZEP520A: anisole = 1:1) for EBL was spin-coated onto the substrate spinning at 3000 rpm for 60 s. Then, the substrate was pre-baked at 180 °C for 2 min. Electrode patterning was performed by EBL (Elionix ELS-7500) and subsequently developed with a ZED-50 N solution. Titanium and platinum (Ti/Pt) electrodes with a thickness of 6/24 nm were deposited on the patterned substrate by sputtering (Miller CFS-4EP-LL). The EBL residue was then removed by dimethyl sulfoxide at 80 °C. Subsequently, the substrate was cleaned with isopropanol and deionized (DI) water under sonication.

The solution of SWNTs/GNRs obtained above was cast around the Ti/Pt electrodes, followed by DEP. The Ti/Pt electrodes were conducted by applying an AC bias voltage for 2 min at different frequencies, ranging from 500 kHz to 15 MHz (33120A Hewlett

Packard Function Generator). The DEP sample was then cleaned with chloroform, dichloroethane, acetone, ethanol, and DI water in that order and subsequently annealed at 200 °C for 1.5 h to remove PmPV, dust, and to increase the adhesion between the GNRs and electrodes. The I-V characteristics of the fabricated samples were measured using a probe system (Pascal Co., Ltd) with a semiconductor parameter analyzer (Agilent 4156B). The fabricated sample was also measured by atomic force microscopy (AFM; JEOL SPM-5200).

3.4. Results and Discussion

Objects are polarized with an inhomogeneous external electric field during DEP. The polarized object generates a side force that moves the object toward higher or lower electric field regions. The DEP force depends on the electric properties of the object and mediums, object size and shape, and the electric field's frequency. The force generated by an electric field E on a dipole with dipole moment p is given by

$$F = (p \cdot \nabla)E \quad . \tag{3.1}$$

In an AC electric field, the time-averaged force on the object is given by

$$F_{DEP} = \Gamma \cdot \varepsilon_m Re\{CM\}\nabla E \quad , \tag{3.2}$$

where Γ is the geometry factor of objects, ε_m is the real part of the permittivity of the medium, and $Re\{CM\}$ is the real part of the Clausius-Mossoti factor, which depends on the complex permittivity and conductivity of the medium and the object[24,28]. For objects elongated in one direction, such as an oblate ellipsoid, carbon nanotubes, and graphene nanoribbons, CM is given by

$$CM = \frac{{\varepsilon_p}^* - {\varepsilon_m}^*}{{\varepsilon_m}^*}, \qquad \varepsilon^* = \varepsilon - i\frac{\sigma}{\omega} \ , \tag{3.3}$$

where the real part of the CM can be described as

$$Re\{CM\} = \frac{\omega^2(\varepsilon_m\varepsilon_p - {\varepsilon_p}^2) + (\sigma_m\sigma_p - {\sigma_m}^2)}{{\varepsilon_m}^2\omega^2 + {\sigma_m}^2} \quad , \tag{3.4}$$

From equations (2) and (4), the sample's DEP force will vary with the electric field and frequency.

Varying AC investigated the electric field's effect in SWNTs/GNRs trapping by DEP applied voltage of function generator. The electric field between 2 electrodes was determined by distance (gap size) and the applied voltage. Electrode with twice gap size will need the twice magnitude of an applied voltage to produce the same volume of an electric field as follow of Coulomb's law principle as state as

$$E_{RMs} = \frac{V_{RMS}}{d} \quad , \tag{3.5}$$

where V_{RMS} is applied voltage in mean root square and d is the distance between 2 electrodes of gap size.

3.4.1. Voltage dependent dielectrophoresis

The Electric field will determine strong or weak attraction and repulsion of DEP force as a state in equation 3.2. We used 1 Vpp, 5 Vpp, and 10 Vpp of AC applied voltage peak to peak during the dielectrophoresis process, which will produce 1.76×10^5 V.m^{-1}, 8.83×10^5 V.m^{-1}, and 1.76×10^5 V.m^{-1} electric field root mean square (E_{RMS}) in 2µm gap size electrode. As shown AFM image of the DEP sample in figure 3.1, the applied AC voltage will determine the number of trapped SWNTs/GNRs. The number of trapped SWNTs/GNRs at 1 Vpp (figure 3.1 (a)) was less than SWNTs/GNRs trapped by 5 Vpp (figure 3.1 (b)) and 10 Vpp (figure 3.1 (c)) applied voltage.

Aligned SWNTs/GNRs quickly form aggregation/kinks with each other during the DEP process caused by attraction and repulsion force between SWNTs/GNRs. With increasing the number of trapped SWNTs/GNRs by increasing applied voltage, the aggregation number also increased. Low applied voltage bias like 1 Vpp was

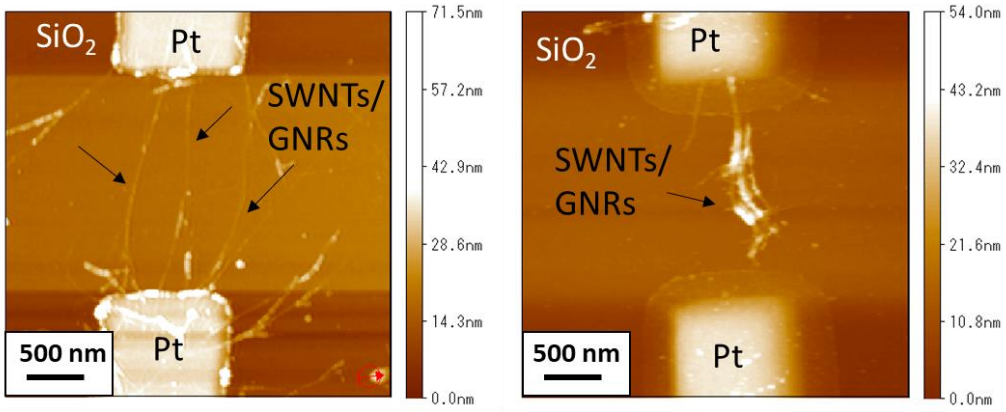

(a) (b)

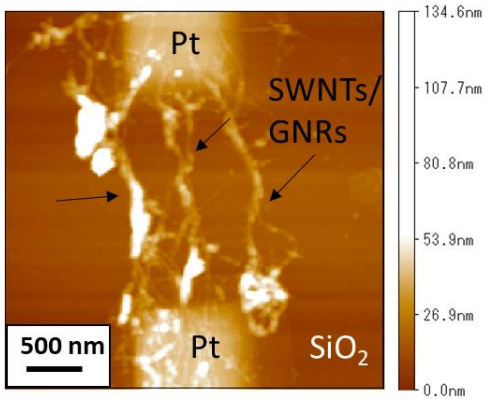

(c)

Figure 3.1. The effect of different applied AC voltage of a. 1 Vpp, b. 5 Vpp and c. 10 Vpp on DEP SWNTs/GNRs with 2µm gap size and 15 MHz frequency.

more suitable to form well-organized or ordered alignment than high applied voltage like 5 Vpp or 10 Vpp.

3.4.2. Frequency dependent dielectrophoresis

Figure 3.2 shows the effect of different frequency DEP in trapping SWNTs/GNRs with a similar electric field and gap size. The number of trapped SWNTs/GNRs was significantly reduced when comparing the DEP result of 0.5 MHz (figure 3.2 (a)) and 5 MHz (figure 3.2 (b)). If we estimate the number trapped SWNTs/GNRs at 0.5 MHz using AFM high for each cluster SWNTs/GNRs in the middle part and divide with average GNRs high and width in AFM (0.6 nm and 3 nm), it will easily reach 6000 GNRs while 5 MHz was only 2000 GNRs. The amount of SWNTs/GNRs trapped in 10 MHz (figure 3.2 (c)) was not much different with 5 MHz, but it reduced to around 500 GNRs when used 15 MHz (figure 3.2 (d)) for frequency DEP

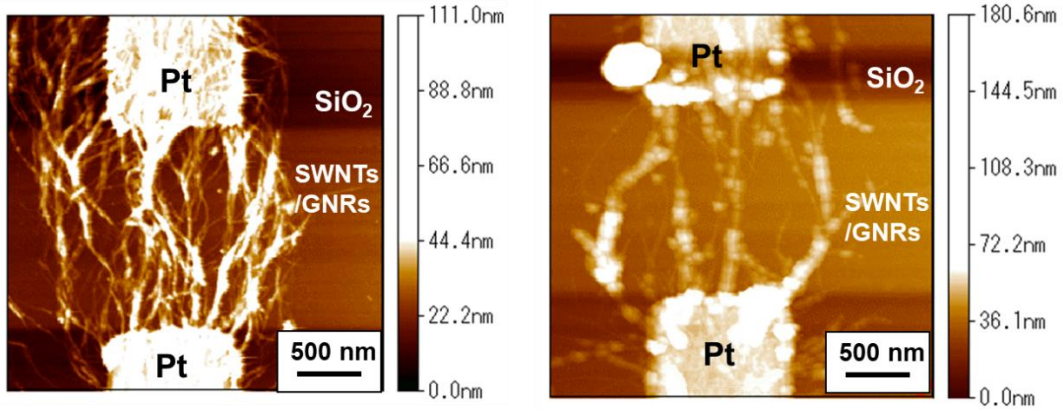

(a) (b)

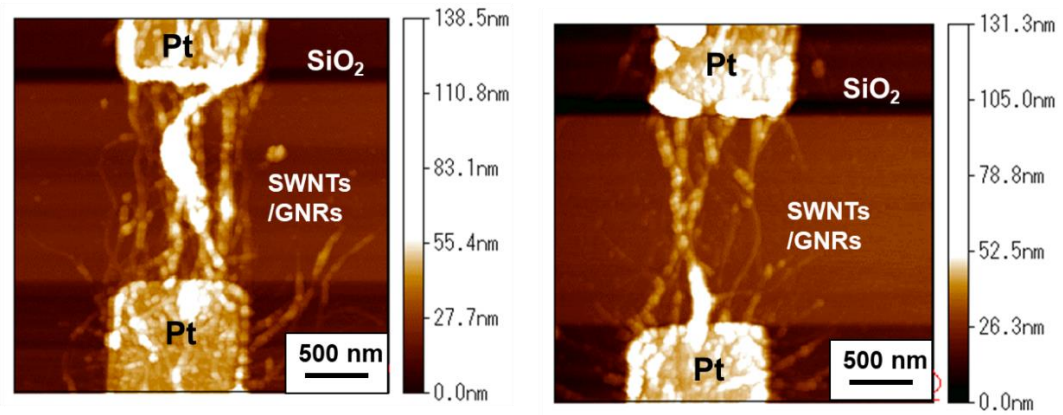

(c) (d)

Figure 3.2. The effect of different frequency of (a) 0.5 MHz, (b) 5 MHz, (c) 10 MHz and (d) 15 MHz on DEP SWNTs/GNRs with 2 μm electrode gap size and 5 Vpp applied voltage

I-V characteristics of trapped SWNTs/GNRs sample for different frequency DEP was shown in figure 3.3. Frequency-dependent DEP was the implication of different conductivity and permittivity SWNTs/GNRs with solvent/medium/dichloroethane as a state in equation 3.4. As metallic SWNTs (mSWNTs) have different conductivity and permittivity values with semiconductor SWNTs (sSWNTs) and GNRs, the DEP force applied to both of them will be different. The I-V curve change from a linear metallic curve to diode like a semiconducting curve may cause trapped sSWNTs/GNRs was more in number than mSWNTs. This result showed the possibility of SWNTs separation with GNRs by frequency-dependent DEP.

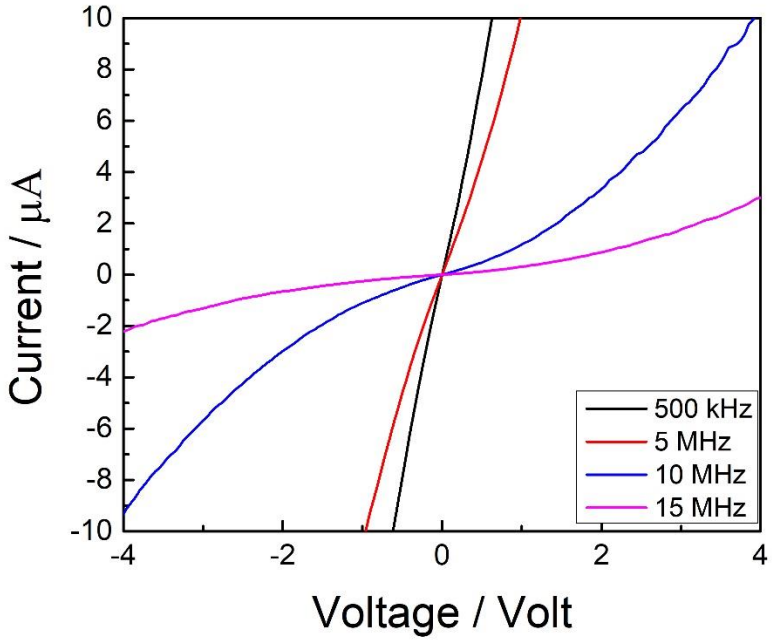

Figure 3.3. I-V characteristics of frequency-dependent DEP

3.4.3. Gap size effect on SWNTs/GNRs dielectrophoresis

The effect of different gap sizes in the same electric field to DEP result was shown in figure 3.4. As shown in figure 3.4, the electrode's gap size influences the way SWNTs/GNRs align. In figure 3.4 (a), because the electrode gap size (1μm) is much less than the average length of SWNTs/GNRs (~1.8μm), the trapped SWNT/GNRs accumulated or folded in between of electrodes. In the case of 2μm gap electrode (figure 3.4 (b)), which has a similar gap size with the average length of SWNTs/GNRs, The SWNTs/GNRs were directly aligned electrode without folding. In the case of 2.5μm gap size, one-side of the trapped SWNTs/GNRs tip was connected to electrode edges when the other end was randomly spread in the gap between the electrode and connected with one or more SWNTs/GNRs. DEP result from gap variation suggests the polarization in a rod-like object such as SWNTs/GNRs accumulate in each tip rather than evenly distribute in all part of an object during DEP which cause of connection

between SWNTs tip with electrode edges, even for easily folded and a thin object like SWNTs/GNRs. This result shows the possibilities of SWNTs/GNRs to form well-ordered serial connections using the appropriate electrode gap size.

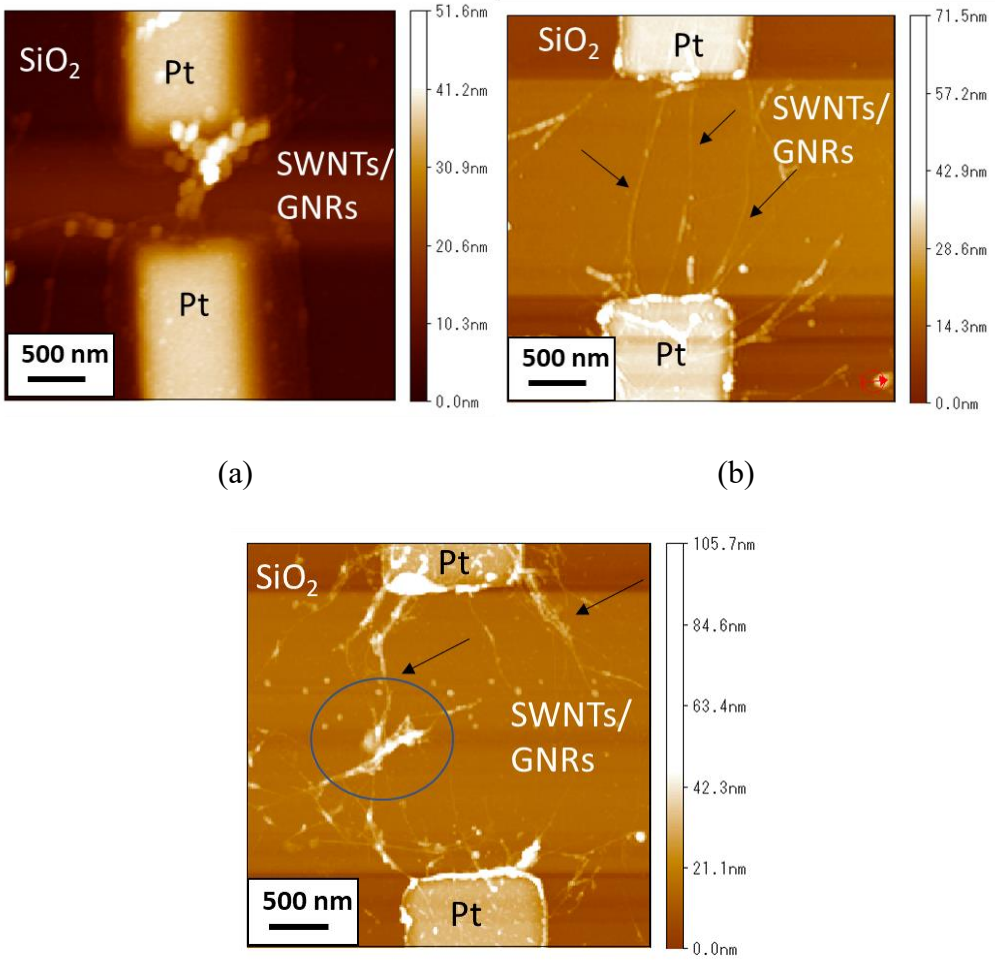

Figure 3.4. The effect of different electrode gap size of a. 1µm, b. 2µm and c. 2.5µm on DEP SWCNTs/GNRs with 8.83×10^5 V/m electric field and 15 MHz frequency

The DEP method described in this work shows the important of voltage, frequency and gap size for alignment and trapping of SWNTs/GNRs. Controllable number of trapped SWNTs/GNRs will possible to achieve with suitable selection of parameter voltage, frequency and gap size.

3.5. Conclusion

In summary, I successfully aligned and assembled SWNTs/GNRs longitudinal unzipping by the DEP method. The increasing applied voltage will increase the amount of trapping while the opposite effect was observed in applied frequency. Besides, the electrode gap size will influence to alignment connection of SWNTs/GNRs. If the electrode gap size is smaller than SWNTs/GNRs length, the SWNTs/GNRs will be folded or accumulated. Otherwise, a double connection will form in alignment. The DEP result for SWNTs/GNRs unzipped form SWNTs HipCo suggested 1 Vpp applied voltage and 15 MHz frequency at 2μm gap size as a suitable parameter for less dense connection.

3.6. Reference

1. Parthasarathy, R., Lin, X.-M. & Jaeger, H. M. Electronic Transport in Metal Nanocrystal Arrays: The Effect of Structural Disorder on Scaling Behavior. *Phys. Rev. Lett.* **87**, 186807 (2001).
2. Marquardt, C. W., Grunder, Sergio., Alfred B., Dehm, S., Hennrich, F., Lo¨hneysen, H. v., Mayor, M. & Krupke, R. Electroluminescence from a single nanotube-molecule-nanotube junction. *Nat. Nanotechnol.* **5**, 863–867 (2010).
3. Ratner, M. A brief history of molecular electronics. *Nat. Nanotechnol.* **8**, 378–381 (2013).
4. Lörtscher, E. Wiring molecules into circuits. *Nat. Nanotechnol.* **8**, 381–384 (2013).
5. Geim, A. K. & Novoselov, K. S. The rise of graphene. *Nat. Mater.* **6**, 183–191 (2007).
6. Bolotin, K. I., Sikes, K. J., Jiang, Z., Klima, M., Fudenberg, G., Hone, J., Kim, P. & Stormer, H. L. Ultrahigh electron mobility in suspended graphene. *Solid State*

Commun. **146**, 351–355 (2008).

7. Han, M. Y., Özyilmaz, B., Zhang, Y. & Kim, P. Energy band-gap engineering of graphene nanoribbons. *Phys. Rev. Lett.* **98**, 206805 (2007).
8. Jacobberger, R. M., Murray, E. A., Fortin-Deschênes, M., Göltl, F., Behn, W. A., Krebs, Z. J., Levesque, P. L., Savage, D. E., Smoot, C., Lagally, M. G., Desjardins, P., Martel, R., Brar, V., Moutanabbir, O., Mavrikakis, M. & Arnold, M. S. Alignment of semiconducting graphene nanoribbons on vicinal Ge(001). *Nanoscale* **11**, 4864–4875 (2019).
9. Fukumori, M., Pandey, R. R., Fujiwara, T., TermehYousefi, A., Negishi, R., Kobayashi, Y., Tanaka, H. & Ogawa, T. Diameter dependence of longitudinal unzipping of single-walled carbon nanotube to obtain graphene nanoribbon. *Jpn. J. Appl. Phys.* **56**, 06GG12 (2017).
10. Fukumori, M., Hara, S., Ogawa, T. & Tanaka, H. Effects of radical initiators, polymerization inhibitors, and other agents on the sonochemical unzipping of double-walled carbon nanotubes. *Jpn. J. Appl. Phys.* **57**, 03ED01 (2018).
11. Tanaka, H., Arima, R., Fukumori, M., Tanaka, D., Negishi, R., Kobayashi, Y., Kasai, S., Yamada, T. K., Ogawa, T. Method for Controlling Electrical Properties of Single-Layer Graphene Nanoribbons via Adsorbed Planar Molecular Nanoparticles. *Sci. Rep.* **5**, 12341 (2015).
12. Pandey, R. R., Fukumori, M., Termehyousefi, A., Eguchi, M., Tanaka, D., Ogawa, T. & Tanaka, H. Tuning the electrical property of a single layer graphene nanoribbon by adsorption of planar molecular nanoparticles. *Nanotechnology* **28**, 175704 (2017).
13. Yamada, T. K., Fukuda, H., Fujiwara, T., Liu, P., Nakamura, K., Kasai, S.,

Vazquez De Parga, A. L. & Tanaka, Hirofumi. Energy gap opening by crossing drop cast single-layer graphene nanoribbons. *Nanotechnology* **29**, 315705 (2018).

14. Kosynkin, D. V., Higginbotham, A. L., Sinitskii, A., Lomeda, J. R., Dimiev, A., Price, B. K. & Tour, J. M. Longitudinal unzipping of carbon nanotubes to form graphene nanoribbons. *Nature* **458**, 872–876 (2009).

15. Cao, J. & Ionescu, A. M. Precise alignment of individual carbon nanotubes for nanoelectronics. in *Proceedings of the IEEE Conference on Nanotechnology* (2012).

16. Santos, M. V. P. dos, Béron, F., Pirota, K. R., Diniz, J. A. & Moshkalev, S. *Electrical Manipulation of a Single Nanowire by Dielectrophoresis*. *Nanowires - New Insights* (2017). doi:10.5772/67386.

17. Shekhar, S., Stokes, P. & Khondaker, S. I. Ultrahigh density alignment of carbon nanotube arrays by dielectrophoresis. *ACS Nano* **5**, 1739–1746 (2011).

18. Boote, J. J. & Evans, S. D. Dielectrophoretic manipulation and electrical characterization of gold nanowires. *Nanotechnology* **16**, 1500–1505 (2005).

19. Raychaudhuri, S., Dayeh, S. A., Wang, D. & Yu, E. T. Precise semiconductor nanowire placement through dielectrophoresis. *Nano Lett.* **9**, 2260–2266 (2009).

20. Freer, E. M., Grachev, O., Duan, X., Martin, S. & Stumbo, D. P. High-yield self-limiting single-nanowire assembly with dielectrophoresis. *Nat. Nanotechnol.* **5**, 525–530 (2010).

21. Dimaki, M. & Bøggild, P. Dielectrophoresis of carbon nanotubes using microelectrodes: A numerical study. *Nanotechnology* **15**, 1095–1102 (2004).

22. Kim, J. E. & Han, C. S. Use of dielectrophoresis in the fabrication of an atomic force microscope tip with a carbon nanotube: A numerical analysis. *Nanotechnology* **16**, 2245–2250 (2005).

CHAPTER 4
Frequency Dependence Dielectrophoresis Technique for Graphene Nanoribbons Separations

4.1. Abstract

We succeeded in bridging unzipped graphene nanoribbons (GNRs) and separating them from unwanted SWNTs using the frequency-dependent dielectrophoresis (DEP) method by varying the frequency and applied voltage used for future assembly. Atomic force micrographs and Raman spectra proved that unzipped GNRs were successfully bridged by the DEP method at frequencies higher than 13 MHz. The theoretical calculation also supported the finding that only GNRs were collected from a mixture of GNRs/SWNT suspensions.

4.2. Introduction

In the past few decades, numerous studies on nanoscale materials for future electronics have been carried out. Nanoscale electrical wiring is one of the biggest challenges for exceeding Moore's law owing to the limitations of fine processing technology in complementary metal-oxide-semiconductors (CMOS)[1-4]. Graphene nanoribbons (GNRs), which are strips of single-atomic layer graphite, have been widely investigated owing to their high electron mobility, mechanical resilience, and high flexibility[5,6]. The electrical properties of GNRs are strongly dependent on their width[7]. When GNRs are more than 10 nm in width, they exhibit semimetallic behavior. On the other hand, when GNRs are less than 10 nm in width, they exhibit semiconductive behavior because their conduction mechanism becomes quasi-one-dimensional, which results in widening of their band-gap. Semiconductive GNRs (sGNRs) are an attractive material for atomic-scale transistor applications[8,9], which are

essential for creating carbon-based molecular circuits. Although there are several approaches to obtain sGNRs[10-12], longitudinal unzipping of carbon nanotubes (CNTs) is one of the most common techniques to obtain sGNRs measuring a few nanometers in width[13,14]. In our previous work, we successfully obtained single-layer sGNRs by the unzipping of single-walled[15-17] and double-walled[18-20] carbon nanotubes (SWNTs and DWNTs) and subsequently carrying out sonication. Although sub-10 nm width sGNRs can be produced by unzipping and are suitable for mass production[13], applying unzipping to the fabrication process of electronic devices remains limited. This is because there is no in-situ method to select only sGNRs from a mixture of unzipped sGNRs and CNTs.

One possible approach of selecting sGNRs from CNTs is the dielectrophoresis (DEP) technique,[21-23] which is the method for nanomaterial alignment that avoids contamination. DEP is applied both in the alignment of nanowires from metal to insulator and in separating materials of differing electrical properties such as metal and semiconductive CNTs (mCNTs and sCNTs, respectively). The separation capability is due to the different DEP forces generated from different conductivities and permittivities in each material[24-29]. These merits indicate that DEP has great potential for solving both the separation problem between sGNRs and CNTs, and the alignment problem between the electrodes by leveraging different materials' responses to the DEP force.

Here, we fabricated sGNRs from SWNTs using the unzipping method. The separated sGNRs were bridged between the micro-gap electrodes during the DEP process allowing separation from the mixture. Frequency dependence was probed by changing the frequency of the applied AC bias voltage between the microgap electrodes.

We succeeded in bridging only sGNRs between electrodes at 13 MHz or higher AC bias voltage because under these conditions the attractive DEP force of the sGNRs becomes stronger than that of SWNTs. This finding was supported by the structural evaluation of bridged SWNTs/sGNRs and theoretical calculations of the DEP process.

4.3. Experimental Procedure

HipCo SWNTs (Nanointegris) were pretreated by annealed at 200 °C for 20 h to remove amorphous carbon, and then acid-treated with HCl (11.65 M at 109 °C) to remove the catalyst metal and induce defects. The GNRs were synthesized by unzipping 0.01 mg of SWNTs using 3 mg poly [(m-phenylenevinylene)-co-(2,5-dioctoxy-p-phenylene-vinylene)] (PmPV; Sigma-Aldrich) in 10 mL dichloroethane solvent. The solution was bath sonicated for 50 min at 37 kHz and 600 W (SHARP UT-606) to initiate the unzipping process. Then, the solution was centrifuged for 16 h at 50,000 G (TOMY Suprema 23 High-Speed Centrifuge) to reduce the remaining SWNTs. The remaining solution (supernatant) was diluted with dichloroethane to reduce the concentration of the mixture SWNTs/GNRs in solution.

Micro-gap electrodes for DEP were fabricated by electron beam lithography (EBL) on a SiO_2 substrate. The residue solution (ZEP520A: anisole = 1:1) for EBL was spin-coated onto the substrate spinning at 3000 rpm for 60 s. Then, the substrate was pre-baked at 180 °C for 2 min. Electrode patterning was performed by EBL (Elionix ELS-7500) and subsequently developed with a ZED-50 N solution. Titanium and platinum (Ti/Pt) electrodes with a thickness of 6/24 nm were deposited on the patterned substrate by sputtering (Miller CFS-4EP-LL). The EBL residue was then removed by dimethyl sulfoxide at 80 °C. Subsequently, the substrate was cleaned with isopropanol and deionized (DI) water under sonication.

The solution of SWNTs/GNRs obtained above was cast around the Ti/Pt electrodes,

followed by DEP. The Ti/Pt electrodes were conducted by applying an AC bias voltage for 2 min at different frequencies, ranging from 500 kHz to 15 MHz (33120A Hewlett Packard Function Generator), as shown in figure 4.1. Then, the DEP sample was cleaned with chloroform, dichloroethane, acetone, ethanol, and DI water in that order and subsequently annealed at 200 °C for 1.5 h to remove PmPV, dust, and to increase the adhesion between the GNRs and electrodes. The I-V characteristics of the fabricated samples were measured using a probe system (Pascal Co., Ltd) with a semiconductor parameter analyzer (Agilent 4156B). The fabricated sample was also measured by atomic force microscopy (AFM; JEOL JSPM-5200) and Raman spectroscopy (Nano Photon Raman Touch) with a 533 nm laser for sample evaluation.

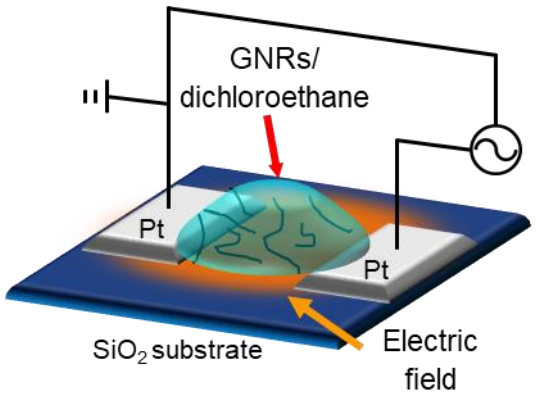

Figure 4.1. Dielectrophoresis Set-up

4.4. Results and Discussion

As shown in Fig, the AC frequency-dependent bridging results of DEP from the SWNT/GNR mixture were observed using AFM. 3.2 and discussed in chapter 3. The change of the I-V curve of frequency dependence DEP suggests a separation between metallic SWNTs and semiconducting SWNTs/GNRs.

Raman spectroscopy of SWNTs' pretreated condition was taken to understand the initial ratio of metallic and semiconducting SWNTs. As shown in figure 4.2 (a) of the

Raman spectrum, pretreated SWNTs contain mixed chirality identified by splitting G band into G^+ and G^-. Also, most of the SWNTs were metallic SWNTs (mSWNTs) shown on the RBM peak in figure 4.2 (b), considering the Kataura-plot[30,31].

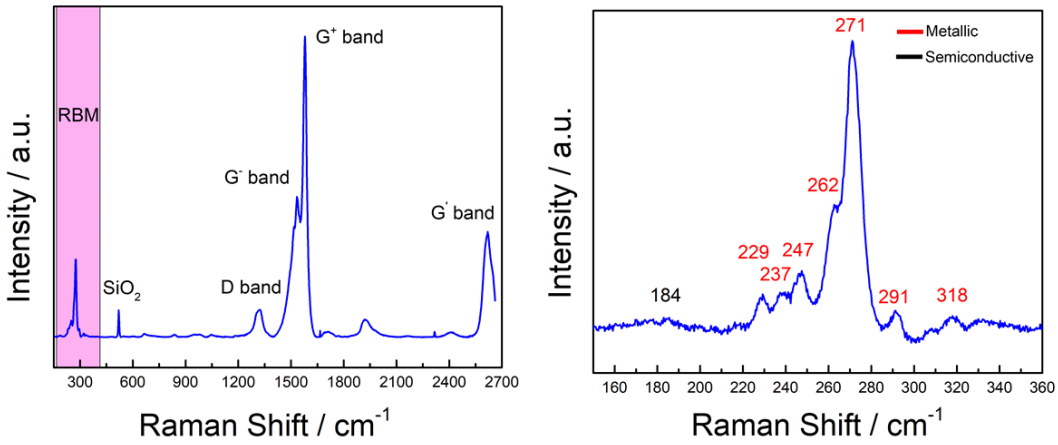

(a) (b)

Figure 4.2 (a) Raman spectrum obtained from initial HipCo SWNTs with inset (b) RBM region shows most composition is mSWNTs.

Separation of SWNTs and GNRs was investigated by varying frequency DEP in the MHz region refer to frequency-dependent result in Chapter 3. To know the boundary for separation of GNRs with excess SWNTs, frequency DEP was varied from 5 MHz to 15 MHz for 1 MHz period.

Confocal Raman microscopy was performed to confirm the type of nanowires bridged between the micro-gap electrodes. Here, possible nanowires were SWNTs and/or GNRs because the presence of D and G band peaks in the Raman spectrum indicate that nanocarbon materials, such as unzipped GNRs and SWNTs, were successfully bridged by DEP, as shown in Fig. 4.4. From the Raman spectra, GNRs and SWNTs can be distinguished by the presence of peaks from the radial breathing mode (RBM). RBM is generated from the stretching in the diameter direction, which means

only SWNTs have this stretching mode. The inset in Fig. 4.4 shows the Raman spectra of the RBM in SiO_2 (substrate), pretreated SWNTs before unzipping, and bridging SWNTs/GNRs with AC bias frequency dependence, respectively. At first, the RBM peaks of pretreated SWNTs before unzipping appeared at approximately 200-300 cm^{-1}, which indicates that the SWNTs were composed mostly of metallic SWNTs (mSWNTs), which suggests that only mSWNTs and sGNRs will remained after the unzipping process. Below 12 MHz, the presence of RBM peaks showed that SWNT residue remains as bridged material by DEP. In contrast, RBM peaks were missing from the sample obtained at frequencies higher than 13 MHz, which indicated that only GNRs can bridge between electrodes. It was proved that only GNRs were successfully separated from a mixture of GNRs with SWNT residue by DEP at frequencies higher than 13 MHz of AC bias.

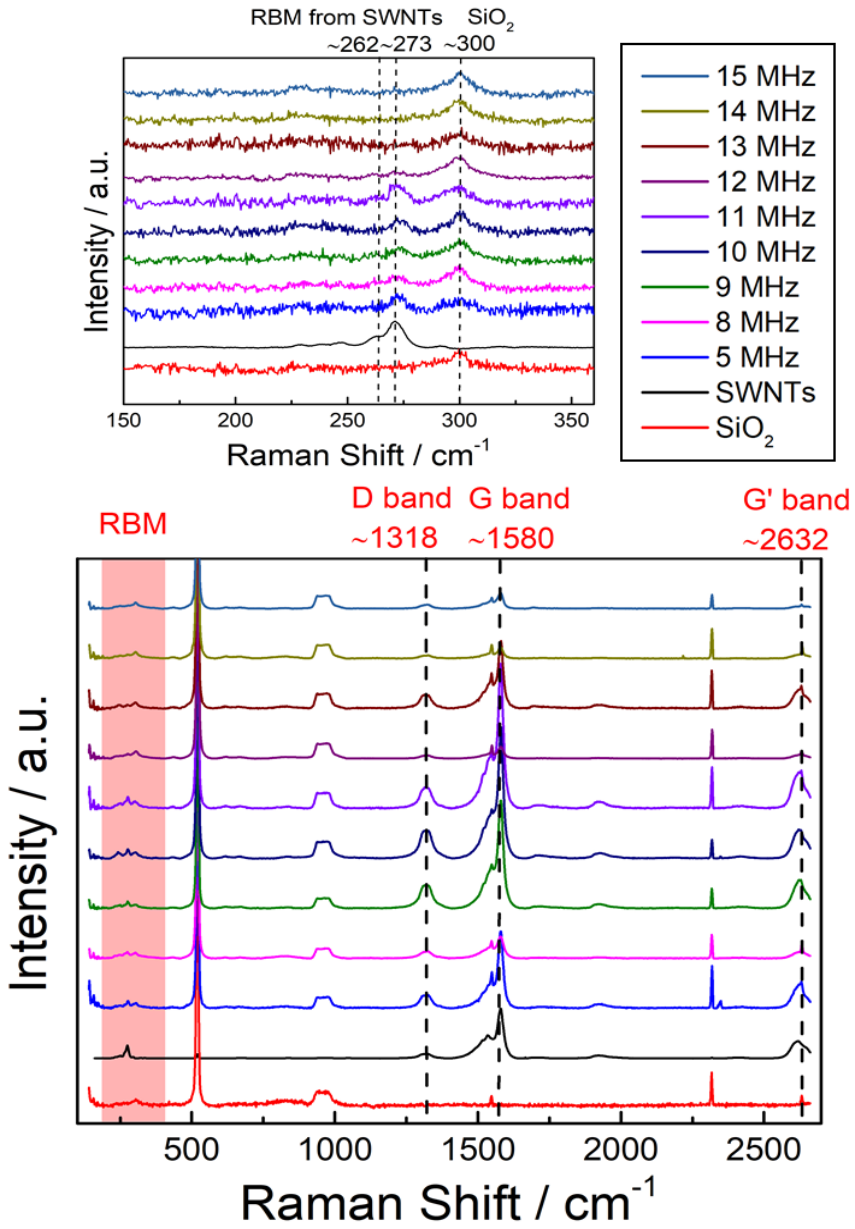

Figure 4.3. Raman spectrum obtained from DEP sample fabricated by varying the frequency of electric field. Black line shows the Raman spectrum of SiO_2 substrate. Red line represents the pretreated SWNTs before unzipping. From peak positions of Raman shift, the starting material is mostly composed by mSWNTs. (Inset) Enlarged Raman spectrum obtained from samples fabricated in higher DEP frequency. In case of 11 and 12 MHz samples, there were peaks of radial breathing modes from mSWNTs.

During the DEP, objects are polarized with an inhomogeneous external electric field. The polarized object generates a side force that moves the object toward higher

or lower electric field regions. The DEP force depends on the electric properties of the object and mediums, object size and shape, and the frequency of the electric field. The force generated by an electric field $\boldsymbol{E}$ on a dipole with dipole moment $\boldsymbol{p}$ is given by

$$F = (p \cdot \nabla)E \quad . \tag{4.1}$$

In an AC electric field, the time-averaged force on the object is given by

$$F_{DEP} = \Gamma \cdot \varepsilon_m Re\{CM\}\nabla E \quad , \tag{4.2}$$

where Γ is the geometry factor of objects, ε_m is the real part of the permittivity of the medium, and $Re\,\{CM\}$ is the real part of the Clausius-Mossoti factor, which depends on the complex permittivity and conductivity of the medium and the object[28,32]. For objects elongated in one direction, such as an oblate ellipsoid, carbon nanotubes, and graphene nanoribbons, CM is given by

$$CM = \frac{{\varepsilon_p}^* - {\varepsilon_m}^*}{{\varepsilon_m}^*}, \qquad \varepsilon^* = \varepsilon - i\frac{\sigma}{\omega} \quad , \tag{4.3}$$

where the real part of the CM can be described as

$$Re\,\{CM\} = \frac{\omega^2\left(\varepsilon_m\varepsilon_p - {\varepsilon_p}^2\right) + \left(\sigma_m\sigma_p - {\sigma_m}^2\right)}{{\varepsilon_m}^2\omega^2 + {\sigma_m}^2} \quad , \tag{4.4}$$

From equations (4.2) and (4.4), the DEP force of the sample will vary with the AC frequency, as shown in Fig. 4. This change in DEP force shows the possibility of separating the excess SWNTs from GNRs to bridge the gap between the micro-gap electrodes.

Bridging by the DEP force will be frequency-dependent as the applied frequency will change the $Re\,\{CM\}$, as stated in equation (4.4). The influence of the conductivity

and permittivity of the medium and object to $Re\ \{CM\}$ in the high- and low-frequency limits is given by

$$Re\{CM\} = \begin{cases} \dfrac{\sigma_p - \sigma_m}{\sigma_m}, & \omega \to 0 \\ \dfrac{\varepsilon_p - \varepsilon_m}{\varepsilon_m}, & \omega \to \infty \end{cases} . \qquad (4.5)$$

where σ_p, σ_m, ε_p, ε_m and are the conductivity of the solute and medium, and the permittivity of the solute and medium, respectively. These values are summarized in Table 1. From the calculation of the limiting value in equation (4.5), there is a crossing point of the frequency-dependent DEP force function from equation (4.2). The inset in Fig. 4 shows that this crossing point is at 34.7 MHz in the positive DEP force region, which indicates that the attractive DEP force of mSWNTs becomes weak compared with that of sGNRs above this frequency. In addition, only sGNRs experience an attractive DEP force in the higher frequency region than the crossing point. This suggests that the amount of bridging sGNRs is greater than the amount of mSWNTs in this frequency region.

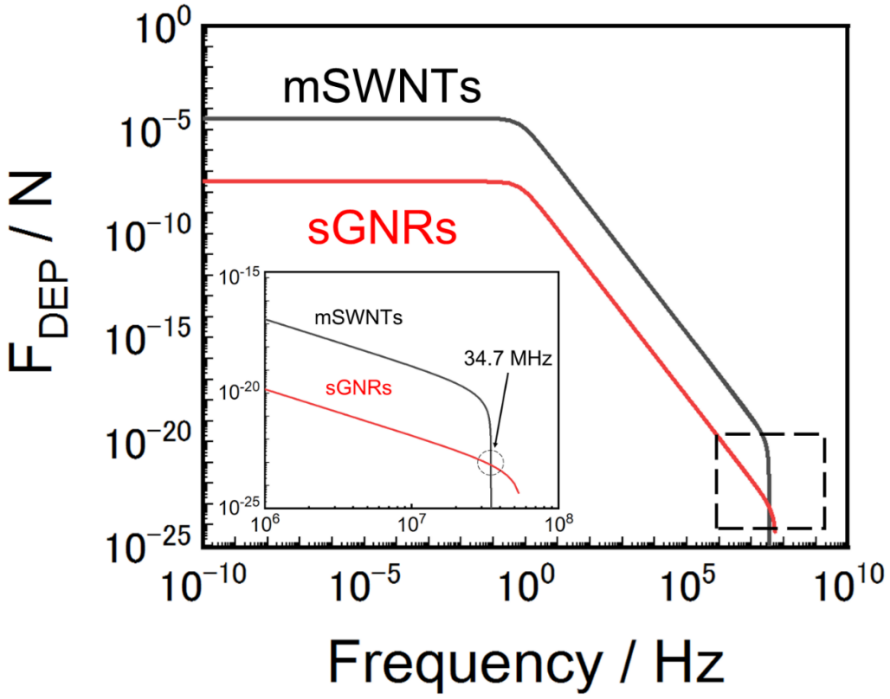

Figure 4.4. Logarithmic plot of frequency dependent DEP force calculation of mSWNTs and sGNRs obtained from equations (2) and (4). A constant electric field is used for easy interpretation. The inset shows the enlarged logarithmic plot of frequency-dependent DEP force in black dot square. Positive DEP force indicates attractive force from electrode gap. The frequency value of crossing point was 34.7 MHz, which indicates that the attractive force of sGNRs becomes stronger than that of mSWNTs.

Table 4.1. Electrical parameter of mSWNTs, sGNRs and dichloroethane. Limit value of DEP force from calculation is included.

Materials	Conductivity ($S \cdot m^{-1}$)	Permittivity ($F \cdot m^{-1}$)	$\frac{\sigma_p - \sigma_m}{\sigma_m}$	$\frac{\varepsilon_p - \varepsilon_m}{\varepsilon_m}$
mSWNTs	1.0×10^{8} (ref.[28])	-8.9×10^{-8} (ref.[28])	2.5×10^{18}	-9.6×10^{2}
sGNRs	9.4×10^{4}	6.1×10^{-11} (ref. [33])	2.4×10^{15}	-3.4×10^{-1}
Dichloroethane	4.0×10^{-11} (ref.[34])	9.3×10^{-11} (ref.[34])	–	–

The phenomenon observed during DEP was considered by comparing the experimental DEP results with the theoretical prediction mentioned earlier. In the lower

frequency region, the conductivity of the object (mSWNTs) is higher than that of the medium, which causes the DEP force to be positive. This positive DEP force pushes the object toward high electric field regions or to the gap between electrodes, as shown in Fig. 2 (a), at 500 kHz. Increasing the applied frequency increases the influence of the object and medium permittivity. The permittivity of the object was lower than that of the medium, which generated a weakened DEP force, moving the object from high electric field regions to lower electric field regions. As the frequency increases, the bridging object between the electrodes is reduced, as observed by AFM (Fig. 2). For frequencies greater than 13 MHz, the DEP force between SWNTs and GNRs was different -SWNTs: repulsive DEP force, GNRs: attractive DEP force - and only GNRs were bridged because of the attractive DEP force. From the experimental results, the frequency of the actual crossing point is estimated to be ~13 MHz, because only sGNRs were obtained at this frequency. The deviation between the theoretical simulations and experimental results occurs because the object shape used in the simulation is only elongated in one direction like an oblate ellipsoid. This can change the crossing point to a lower frequency owing to the shape of the GNR being strips of one atomic layer thickness carbon. The order of the experimental value coincides with the calculation value, which suggests that the experiment and calculation are consistent with each other when it comes to generated forces.

4.5. Conclusion

In summary, we fabricated sGNRs from mSWNTs by the unzipping method and investigated the separation of sGNRs from a mixture of mSWNT residue by the DEP technique by changing the frequency of the applied AC bias voltage between the micro-gap electrodes. From the structural and electrical evaluation of bridging mSWNTs/sGNRs, we successfully obtained bridging sGNRs without mSWNTs

between electrodes at 13 MHz or higher AC bias voltage. Theoretical calculations suggest that the repulsive DEP force from the electrodes in the mSWNTs becomes stronger than that in the sGNRs at 10^7 Hz or more, which separates sGNRs between electrodes in this frequency region. The separation of single-layer-level sGNRs from SWNTs is achieved via the DEP method. This is a promising discovery in the study of nanoscale material electronics application

4.6. Reference

1. Parthasarathy, R., Lin, X.-M. & Jaeger, H. M. Electronic Transport in Metal Nanocrystal Arrays: The Effect of Structural Disorder on Scaling Behavior. *Phys. Rev. Lett*. **87**, 186807 (2001).
2. Marquardt, C. W., Grunder, Sergio., Alfred B., Dehm, S., Hennrich, F., Lo¨hneysen, H. v., Mayor, M. & Krupke, R. Electroluminescence from a single nanotube-molecule-nanotube junction. *Nat. Nanotechnol*. **5**, 863–867 (2010).
3. Ratner, M. A brief history of molecular electronics. *Nat. Nanotechnol*. **8**, 378–381 (2013).
4. Lörtscher, E. Wiring molecules into circuits. *Nat. Nanotechnol.* **8**, 381–384 (2013).
5. Geim, A. K. & Novoselov, K. S. The rise of graphene. *Nat. Mater.* **6**, 183–191 (2007).
6. Bolotin, K. I., Sikes, K. J., Jiang, Z., Klima, M., Fudenberg, G., Hone, J., Kim, P. & Stormer, H. L. Ultrahigh electron mobility in suspended graphene. *Solid State Commun.* **146**, 351–355 (2008).
7. Han, M. Y., Özyilmaz, B., Zhang, Y. & Kim, P. Energy band-gap engineering of graphene nanoribbons. *Phys. Rev. Lett.* **98**, 206805 (2007).

8. Suzuki, H., Kaneko, T., Shibuta, Y., Ohno, M., Maekawa, Y. & Kato, T. Wafer-scale fabrication and growth dynamics of suspended graphene nanoribbon arrays. *Nat. Commun.* **7**, 11797 (2016).

9. Jacobberger, R. M., Murray, E. A., Fortin-Deschênes, M., Göltl, F., Behn, W. A., Krebs, Z. J., Levesque, P. L., Savage, D. E., Smoot, C., Lagally, M. G., Desjardins, P., Martel, R., Brar, V., Moutanabbir, O., Mavrikakis, M. & Arnold, M. S. Alignment of semiconducting graphene nanoribbons on vicinal Ge(001). *Nanoscale* **11**, 4864–4875 (2019)

10. Wang, X. & Dai, H. Etching and narrowing of graphene from the edges. *Nat. Chem.* **2**, 661–665 (2010).

11. Liu, L., Zhang, Y., Wang, W., Gu, C., Bai, X. & E. Wang, Nanosphere Lithography for the Fabrication of Ultranarrow Graphene Nanoribbons and On-Chip Bandgap Tuning of Graphene. *Adv. Mater*. **23** [10], 1246–1251 (2011).

12. J. Yamaguchi, H. Hayashi, H. Jippo, A. Shiotari, M. Ohtomo, M. Sakakura, N. Hieda, N. Aratani, M. Ohfuchi, Y. Sugimoto, H. Yamada & S. Sato. Small bandgap in atomically precise 17-atom-wide armchair-edged graphene nanoribbons. *Commun. Mater.* **1** [36], 1-9 (2020).

13. Kosynkin, D. V., Higginbotham, A. L., Sinitskii, A., Lomeda, J. R., Dimiev, A., Price, B. K. & Tour, J. M. Longitudinal unzipping of carbon nanotubes to form graphene nanoribbons. *Nature* **458**, 872–876 (2009).

14. Wei, D., Xie, L., Lee, K. K., Hu, Z., Tan, S., Chen, W., Sow, C. H., Chen, K., Liu, Y. & Wee, A. T. S. Controllable unzipping for intramolecular junctions of graphene nanoribbons and single-walled carbon nanotubes. *Nat. Commun.* **4**, 1374 (2013).

15. Fukumori, M., Pandey, R. R., Fujiwara, T., TermehYousefi, A., Negishi, R., Kobayashi, Y., Tanaka, H. & Ogawa, T. Diameter dependence of longitudinal unzipping of single-walled carbon nanotube to obtain graphene nanoribbon. *Jpn. J. Appl. Phys.* **56**, 06GG12 (2017).

16. Furuki, H., Fujiwara, T., TermehYousefi, A. & Tanaka, H. Sequential experimental strategies of longitudinal unzipping of SWNTs: Selective width of single layer graphene nanoribbon. *Proceedings of the 2017 11th IEEE Regional Symposium on Micro and Nanoelectronics* 8069173, 171-174 (2017).

17. Fukumori, M., Hara, S., Ogawa, T. & Tanaka, H. Effects of radical initiators, polymerization inhibitors, and other agents on the sonochemical unzipping of double-walled carbon nanotubes. *Jpn. J. Appl. Phys*. **57**, 03ED01 (2018).

18. Tanaka, H., Arima, R., Fukumori, M., Tanaka, D., Negishi, R., Kobayashi, Y., Kasai, S., Yamada, T. K. & Ogawa, T. Method for Controlling Electrical Properties of Single-Layer Graphene Nanoribbons via Adsorbed Planar Molecular Nanoparticles. *Sci. Rep.* **5**, 12341 (2015).

19. Pandey, R. R., Fukumori, M., Termehyousefi, A., Eguchi, M., Tanaka, D., Ogawa, T. & Tanaka, H. Tuning the electrical property of a single layer graphene nanoribbon by adsorption of planar molecular nanoparticles. *Nanotechnology* **28**, 175704 (2017).

20. Yamada, T. K., Fukuda, H., Fujiwara, T., Liu, P., Nakamura, K., Kasai, S., Vazquez De Parga, A. L. & Tanaka, H. Energy gap opening by crossing drop cast single-layer graphene nanoribbons. *Nanotechnology* **29**, 315705 (2018).

21. Cao, J., & Ionescu, A. M. Precise alignment of individual carbon nanotubes for nanoelectronics. *Proceedings of the 12th IEEE Conference on Nanotechnology*, 1-5 (2012).

22. Puydinger dos Santos, M. V., Béron, F., Pirota, K. R., Diniz, J. A. & Moshkalev, S. Electrical Manipulation of a Single Nanowire by Dielectrophoresis, *Nanowires - New Insights, Khan Maaz, IntechOpen* (2017).

23. Shekhar, S., Stokes, P. & Khondaker, S. I. Ultrahigh density alignment of carbon nanotube arrays by dielectrophoresis. *ACS Nano* **5** [3], 1739–1746 (2011).

24. Boote, J. J. & Evans, S. D. Dielectrophoretic manipulation and electrical characterization of gold nanowires. *Nanotechnology* **16** [9], 1500–1505 (2005).

25. Raychaudhuri, S., Dayeh, S. A., Wang, D. & Yu, E. T. Precise semiconductor nanowire placement through dielectrophoresis. *Nano Lett.* **9**, 2260–2266 (2009).

26. Freer, E. M., Grachev, O., Duan, X., Martin, S. & Stumbo, D. P. High-yield self-limiting single-nanowire assembly with dielectrophoresis. *Nat. Nanotechnol.* **5**, 525–530 (2010).

27. Puydinger dos Santos, M. V., Lima, L. P. B., Mayer, R. A., Béron, F., Pirota, K. R. & Diniz, J. A. Dielectrophoretic manipulation of individual nickel nanowires for electrical transport measurements. *J. Vac. Sci. Technol. B, Nanotechnol. Microelectron. Mater. Process. Meas. Phenom.* **33** [3], 031804 (2015).

28. Dimaki, M. & Bøggild, P. Dielectrophoresis of carbon nanotubes using microelectrodes: A numerical study. *Nanotechnology* **15**, 1095–1102 (2004).

29. Mendes, M. J., Schmidt, H. K. & Pasquali, M. Brownian dynamics simulations of single-wall carbon nanotube separation by type using dielectrophoresis. *J. Phys. Chem. B* **112** [25], 7467-7477 (2008).

30. Kataura, H., Kumazawa, Y., Maniwa, Y., Umezu, I., Suzuki, S., Ohtsuka, Y. & Achiba, Y. Optical properties of oxidized single-wall carbon nanotubes. *Synth. Met.* **103**, 2555-2558 (1999).

31. Cheng, Q., Debnath, S., Gregan, E. & Byrne, H. J. Vibrational mode assignments for bundled single-wall carbon nanotubes using Raman spectroscopy at different excitation energies. *Appl. Phys. A Mater. Sci. Process.* **102** [2], 309 -317 (2011).

32. Kim, J. E. & Han, C. S. Use of dielectrophoresis in the fabrication of an atomic force microscope tip with a carbon nanotube: A numerical analysis. *Nanotechnology* **16** [10], 2245-2250 (2005).

33. Fang, J., Vandenberghe, W. G. & Fischetti, M. V. Microscopic dielectric permittivities of graphene nanoribbons and graphene. *Phys. Rev. B* **94** [4], 045318 (2016).

34. I. M. Smallwood. Handbook of Organic Solvent Properties. *Butterworth-Heinemann*, (1996).

CHAPTER 5

Single Trapping Graphene Nanoribbons Unzipped Single-Walled Carbon Nanotubes by Dielectrophoresis

5.1. Abstract

We successfully trapped and align single-layer graphene nanoribbons (s-GNRs) obtain from mechanical longitudinal unzipping. 1 Vpp applied voltage, 15 MHz frequency, 2 μm gap size, and 50 times dilution of supernatant were used as DEP parameters to produce 2 μm s-GNRs alignment. The AFM analysis, RBM Raman spectrum, and I-V characteristic was used to prove the trapping material was GNRs.

5.2. Introduction

Graphene nanoribbons (GNRs) has attracted attention of semiconductor technologies due to possibility in opening band-gap. The value of GNR band-gap was inversely proportional with ribbons width[1]. Even though there are several approaches to obtain sGNRs[2,3], longitudinal unzipping of carbon nanotubes (CNTs) is one of the most promising techniques to obtain sGNRs measuring a few nanometers in width with smooth edges[4,5]. In our previous work, we successfully obtained single-layer sGNRs by the unzipping of single-walled[6,7] and double-walled[8-10] carbon nanotubes (SWNTs and DWNTs) and subsequently carrying out sonication. Although sub-10 nm width sGNRs can be produced by unzipping and are suitable for mass production[11], applying unzipping to the fabrication process of electronic devices remains limited. This is because there is no in-situ method to select only sGNRs from a mixture of unzipped sGNRs and CNTs.

One possible approach of selecting sGNRs from CNTs is the dielectrophoresis (DEP) technique[12,13] which is the method for nanomaterial alignment that avoids

contamination. DEP is applied both in the alignment of nanowires from metal to insulator and in separating materials of differing electrical properties such as metal and semiconductive CNTs (mCNTs and sCNTs, respectively). The separation capability is due to the different DEP forces generated from different conductivities and permittivities in each material[11,14-16]. These merits indicate that DEP has excellent potential for solving both the separation problem between sGNRs and CNTs and the alignment problem between the electrodes by leveraging different materials responses to the DEP force. Even though DEP was already used in CNTs[13,17,18] and other materials[11,19] but the capabilities to produce single-layer trapping for nanomaterial such as CNTs, and GNRs have not yet proven.

Here, we succeeded in proving since trapping by DEP technique with GNRs obtain from the unzipping method of SWNTs.

5.3. Experimental Procedure

HipCo SWNTs (Nanointegris) were pretreated by annealed at 200 °C for 20 h to remove amorphous carbon, and then acid-treated with HCl (11.65 M at 109 °C) to remove the catalyst metal and induce defects. The GNRs were synthesized by unzipping 0.01 mg of SWNTs using 3 mg poly [(m-phenylenevinylene)-co-(2,5-dioctoxy-p-phenylene-vinylene)] (PmPV; Sigma-Aldrich) in 10 mL dichloroethane solvent. The solution was bath sonicated for 50 min at 37 kHz and 600 W (SHARP UT-606) to initiate the unzipping process. Then, the solution was centrifuged for 16 h at 50,000 G (TOMY Suprema 23 High-Speed Centrifuge) to reduce the remaining SWNTs. The remaining solution (supernatant) was diluted with dichloroethane to reduce the concentration of the mixture SWNTs/GNRs in solution.

Micro-gap electrodes for DEP were fabricated by electron beam lithography (EBL) on a SiO_2 substrate. The residue solution (ZEP520A: anisole = 1:1) for EBL was spin-

coated onto the substrate spinning at 3000 rpm for 60 s. Then, the substrate was pre-baked at 180 °C for 2 min. Electrode patterning was performed by EBL (Elionix ELS-7500) and subsequently developed with a ZED-50 N solution. Titanium and platinum (Ti/Pt) electrodes with a thickness of 6/24 nm were deposited on the patterned substrate by sputtering (Miller CFS-4EP-LL). The EBL residue was then removed by dimethyl sulfoxide at 80°C. Subsequently, the substrate was cleaned with isopropanol and deionized (DI) water under sonication.

The solution of SWNTs/GNRs obtained above was cast around the Ti/Pt electrodes, followed by DEP. The Ti/Pt electrodes were conducted by applying 1 Vpp AC bias voltage for 2 min at different frequency 15 MHz (33120A Hewlett Packard Function Generator). Then, the DEP sample was cleaned with chloroform, dichloroethane, acetone, ethanol, and DI water in that order and subsequently annealed at 200 °C for 1.5 h to remove PmPV, dust, and to increase the adhesion between the GNRs and electrodes. The I-V characteristics of the fabricated samples were measured using a probe system (Pascal Co., Ltd) with a semiconductor parameter analyzer (Agilent 4156B). The fabricated sample was also measured by atomic force microscopy (AFM; JEOL JSPM-5200) and Raman spectroscopy (Nano Photon Raman Touch) with a 533 nm laser for sample evaluation.

5.4. Results and Discussion

As discussed in chapter 3 and 4, the number of trapped SWNTs/GNRs by the DEP method can be adjusted using applied voltage and frequency. In this work, 1 Vpp applied voltage, 15 MHz frequency, 2 μm gap size, and 50 times ratio dilution supernatant to produce single GNRs trapping. Figure 5.1 (a) shown the result of successfully trapped GNRs, which contains two aligned GNRs. The height of GNRs

shown in enlarge version figure 5.1 (b) was less than 1µm, which is the average height of SWNTs by AFM and Raman SWNTs RBM by Raman in chapter 4.

For further investigation, the Raman spectrum and imaging were measured using Raman spectroscopy. Figure 5.2 (a) shows the AFM image of the Raman sample and area around the black dash line, which contains GNRs according to Raman imaging shows on 5.2 (c) yellow dash line. In Raman imaging, each pixel represents a 500 nm area of scanning. The meaning of a pixel's bright color was correlated to the intensity of scanned wavenumber, resulting in stronger intensity with a brighter pixel's color.

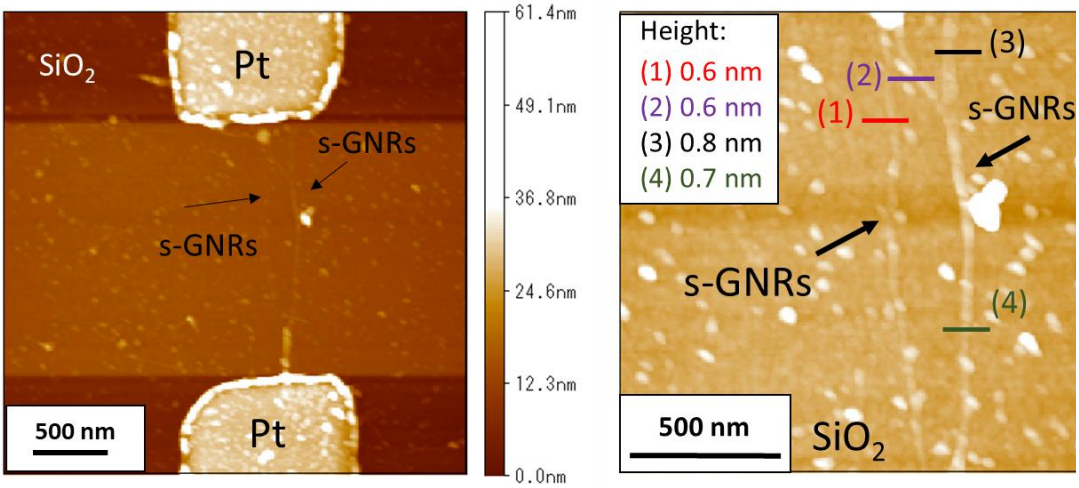

(a) (b)

Figure 5.1. (a) AFM image of 2 GNRs trapped by DEP method with the height of s-GNRs shown by (b) enlarge version.

Figure 5.3 (a) shows the presence of D and G band, and 5.3 (b) confirm the absence of RBM peak SWNTs in 8 pixels enclosed by the yellow dash line in 5.3 (c). This result was confirmation of s-GNRs material was present in the DEP sample. Besides, I-V characteristics of the s-GNRs in figure 5.4 shown proper connection was form between s-GNRs and Pt electrode. The I-V curve was a non-linear I-V curve that typically

appears in diode like semiconductor material. DEP alignment was conducted with the same DEP parameter. AFM image from the DEP result with the same parameter was shown in figure 5.5 (a) and (b).in order to check repeatability to reproduce s-GNRs connections. The connection of s-GNRs was formed successfully with only s-GNR connected between both electrodes, which show the DEP technique's repeatability.The successfully trappings-GNRs in this research showed the DEP technique's capability to align and assembly s-GNRs for GNRs electronics devices fabrications.

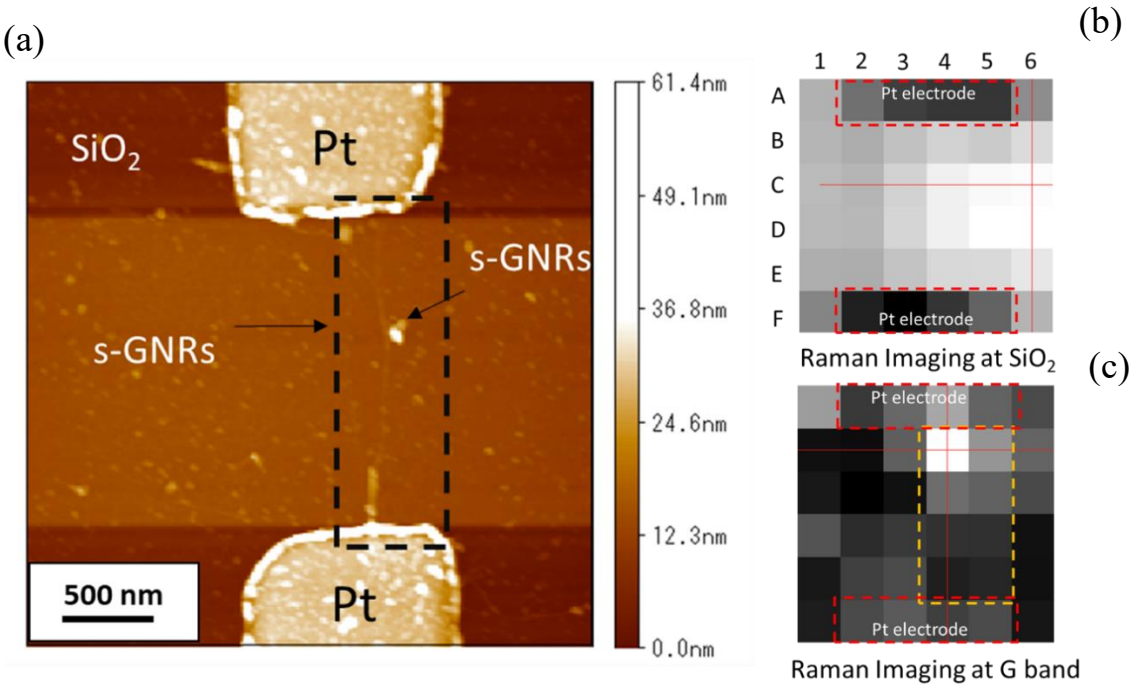

Figure 5.2. (a) AFM image shows Raman imaging spectrum area of 2 bridging s-GNRs where (b) Raman imaging at SiO_2 (Raman shift: 520 cm^{-1}) and (c) G band (Raman shift: 1580 cm^{-1}) scanned.

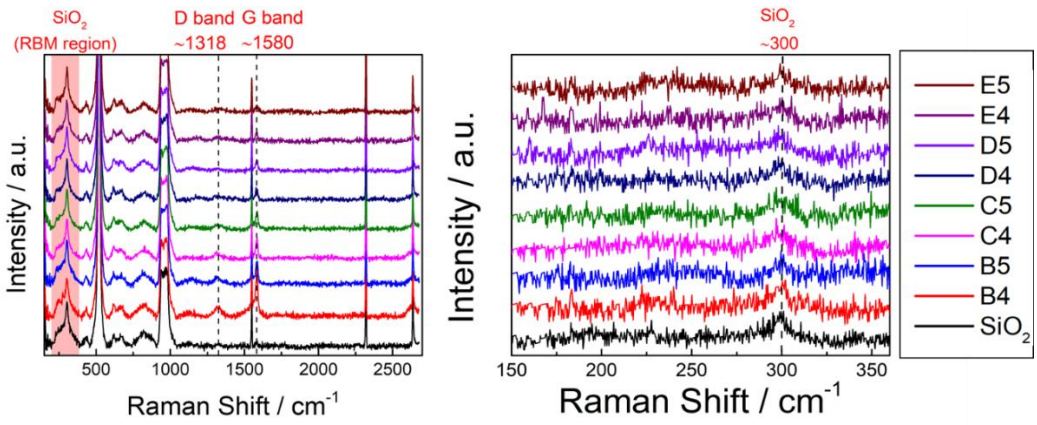

(a) (b)

Figure 5.3. Raman spectra from imaging in 8 pixels as shown in Fig.5.3 (c). Owing to the presence of D and G band (a) and absence of RBM as shown in enlarge version (b), these Raman spectra originated from sGNRs

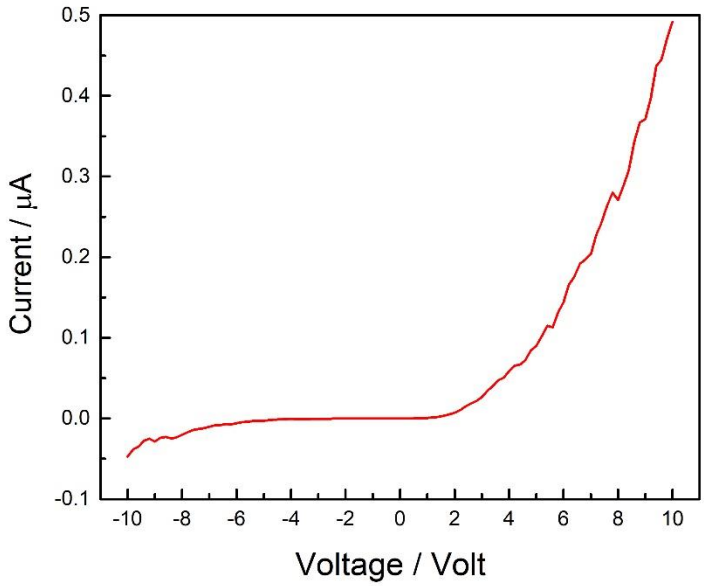

Figure 5.4. I-V characteristics of trapped s-GNRs by DEP technique

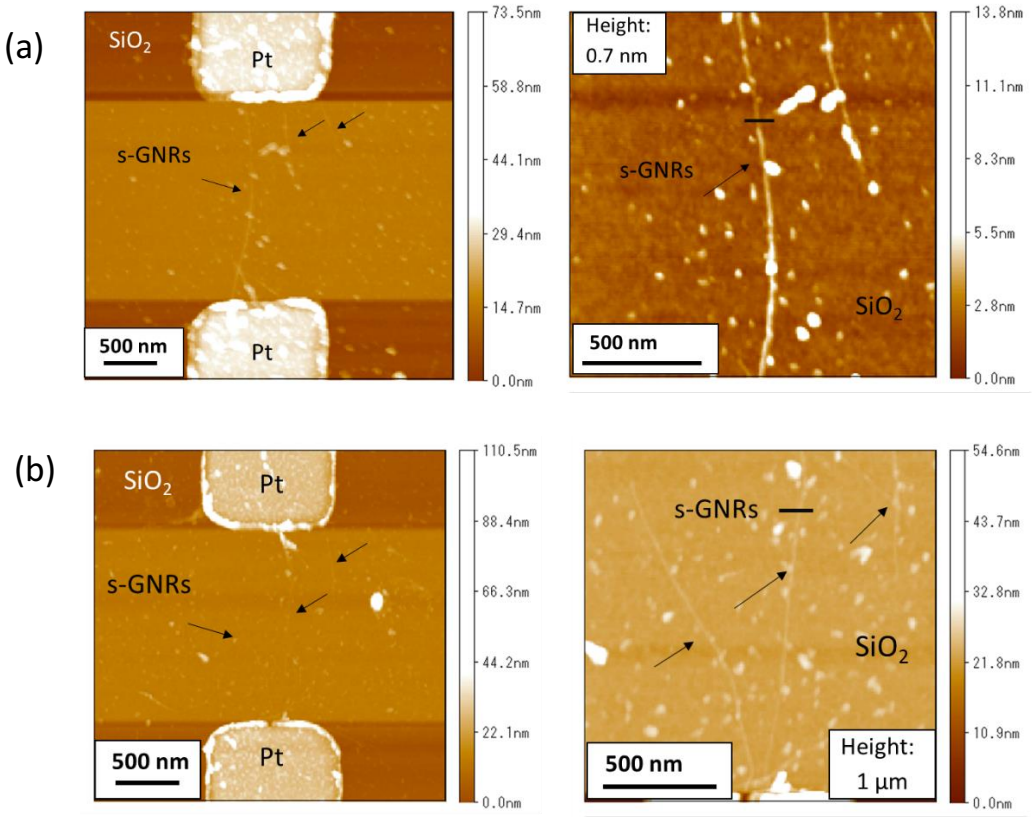

Figure 5.5. AFM images of the DEP results with the same DEP parameters to know the repeatability s-GNRs trapping. Both (a) and (b) produced only 1 s-GNRs which shows the repeatability of the DEP parameters.

5.5. Conclusion

In summary, s-GNRs only trapping was successfully conducted using the DEP technique. 1 Vpp applied voltage, 15 MHz frequency, 2µm gap size, and 50 times ratio dilution supernatant was used as the DEP parameter. The AFM analysis and RBM spectrum data prove the material trapped was s-GNRs. I-V characteristics show semiconducting I-V curves. The DEP parameter's repeatability to produce s-GNRs trapping was shown by the other 2 AFM images in DEP process.

5.6. Reference

1. Han, M. Y., Özyilmaz, B., Zhang, Y. & Kim, P. Energy band-gap engineering of

graphene nanoribbons. *Phys. Rev. Lett.* **98**, 206805 (2007).

2. Wang, X. & Dai, H. Etching and narrowing of graphene from the edges. *Nat. Chem.* **2**, 661–665 (2010).
3. Liu, L., Zhang, Y., Wang, W., Gu, C., Bai, X. & E. Wang, Nanosphere Lithography for the Fabrication of Ultranarrow Graphene Nanoribbons and On-Chip Bandgap Tuning of Graphene. *Adv. Mater*. **23** [10], 1246–1251 (2011).
4. Kosynkin, D. V., Higginbotham, A. L., Sinitskii, A., Lomeda, J. R., Dimiev, A., Price, B. K. & Tour, J. M. Longitudinal unzipping of carbon nanotubes to form graphene nanoribbons. *Nature* **458**, 872–876 (2009).
5. Wei, D., Xie, L., Lee, K. K., Hu, Z., Tan, S., Chen, W., Sow, C. H., Chen, K., Liu, Y. & Wee, A. T. S. Controllable unzipping for intramolecular junctions of graphene nanoribbons and single-walled carbon nanotubes. *Nat. Commun.* **4**, 1374 (2013).
6. Fukumori, M., Pandey, R. R., Fujiwara, T., TermehYousefi, A., Negishi, R., Kobayashi, Y., Tanaka, H. & Ogawa, T. Diameter dependence of longitudinal unzipping of single-walled carbon nanotube to obtain graphene nanoribbon. *Jpn. J. Appl. Phys.* **56**, 06GG12 (2017).
7. Fukumori, M., Hara, S., Ogawa, T. & Tanaka, H. Effects of radical initiators, polymerization inhibitors, and other agents on the sonochemical unzipping of double-walled carbon nanotubes. *Jpn. J. Appl. Phys.* **57**, 03ED01 (2018).
8. Tanaka, H., Arima, R., Fukumori, M., Tanaka, D., Negishi, R., Kobayashi, Y., Kasai, S., Yamada, T. K., Ogawa, T. Method for Controlling Electrical Properties of Single-Layer Graphene Nanoribbons via Adsorbed Planar Molecular Nanoparticles. *Sci. Rep.* **5**, 12341 (2015).
9. Pandey, R. R., Fukumori, M., Termehyousefi, A., Eguchi, M., Tanaka, D., Ogawa, T. & Tanaka, H. Tuning the electrical property of a single layer graphene

nanoribbon by adsorption of planar molecular nanoparticles. *Nanotechnology* **28**, 175704 (2017).

10. Yamada, T. K., Fukuda, H., Fujiwara, T., Liu, P., Nakamura, K., Kasai, S., Vazquez De Parga, A. L. & Tanaka, Hirofumi. Energy gap opening by crossing drop cast single-layer graphene nanoribbons. *Nanotechnology* **29**, 315705 (2018).
11. Boote, J. J. & Evans, S. D. Dielectrophoretic manipulation and electrical characterization of gold nanowires. *Nanotechnology* **16**, 1500–1505 (2005).
12. Puydinger dos Santos, M. V., Béron, F., Pirota, K. R., Diniz, J. A. & Moshkalev, S. Electrical Manipulation of a Single Nanowire by Dielectrophoresis, *Nanowires - New Insights, Khan Maaz, IntechOpen* (2017).
13. Shekhar, S., Stokes, P. & Khondaker, S. I. Ultrahigh density alignment of carbon nanotube arrays by dielectrophoresis. *ACS Nano* **5**, 1739–1746 (2011).
14. Raychaudhuri, S., Dayeh, S. A., Wang, D. & Yu, E. T. Precise semiconductor nanowire placement through dielectrophoresis. *Nano Lett.* **9**, 2260–2266 (2009).
15. Freer, E. M., Grachev, O., Duan, X., Martin, S. & Stumbo, D. P. High-yield self-limiting single-nanowire assembly with dielectrophoresis. *Nat. Nanotechnol.* **5**, 525–530 (2010).
16. Dimaki, M. & Bøggild, P. Dielectrophoresis of carbon nanotubes using microelectrodes: A numerical study. *Nanotechnology* **15**, 1095–1102 (2004).
17. Le Louarn, A., Kapche, F., Bethoux, J. M., Happy, H., Dambrine, G.,Derycke, V., Chenevier, P., Izard, N., Goffman, M. F. & Bourgoin, J. P. Intrinsic current gain cutoff frequency of 30 GHz with carbon nanotube transistors. *Appl. Phys. Lett.* **90**, 3–6 (2007).
18. Kim, J. E. & Han, C. S. Use of dielectrophoresis in the fabrication of an atomic force microscope tip with a carbon nanotube: A numerical analysis.

Nanotechnology **16**, 2245–2250 (2005).

19. Puydinger dos Santos, M. V., Lima, L. P. B., Mayer, R. A., Béron, F., Pirota, K. R. & Diniz, J. A. Dielectrophoretic manipulation of individual nickel nanowires for electrical transport measurements. *J. Vac. Sci. Technol. B, Nanotechnol. Microelectron. Mater. Process. Meas. Phenom.* **33** [3], 031804 (2015).

CHAPTER 6
Conclusions and Suggestions

In conclusions, graphene nanoribbons (GNRs) with excess single-walled carbon nanotubes (SWNTs) was successfully align and assembly by the dielectrophoresis (DEP) method. The effect of DEP parameters such as applied voltage, frequency, and gap size into the amount and alignment of trapped SWNTs/GNRs was investigated. The number of trapped SWNTs/GNRs increased with increasing applied voltage, and the opposite effect appears in applied frequency. The DEP electrode's gap size will affect the alignment form of trapped SWTs/GNRs, which are related to the SWNTs/GNRs length.

The GNRs were also successfully separated from excess SWNTs by frequency dependence DEP. The RBM Raman spectra, AFM image, and DEP force calculations serve as proof of only GNRs trapped with more 13 MHz applied frequency. Single-layer GNRs (s-GNRs) were also successfully trapped and align by adjusting the DEP parameter to 1 Vpp applied voltage, 15 MHz frequency, 2 μm gap size, and 50 times dilution of supernatant. The trapping s-GNRs was proved repeatable with similar parameter.

The are several devices that can be fabricated with this result, such as FET and sensor. On the other hand, fines control of number GNRs trapping and stacking trapped GNRs using multiple electrodes also interesting for a future experiment.

LIST OF PUBLICATION

Wahyu Waskito Aji, Yuki Usami, Hadiyawarman, Rikuto Oyabu, and Hirofumi Tanaka, "Frequency dependence dielectrophoresis technique for bridging graphene nanoribbons", *Applied Physics Express* **13**, 101004 (2020)

LIST OF CONFERENCE

ORAL PRESENTATION

1. **Wahyu Waskito Aji**, Hirofumi Tanaka., "Study of Trapping Condition on Dielectrophoresis to Fabricate GNRs Devices", International Symposium of Applied Science (ISAS) 2019, Ho Chi Minh City -Vietnam.
2. **Wahyu Waskito Aji**, Yuki Usami, Hadiyawarman, Rikuto Oyabu, and Hirofumi Tanaka, "Frequency dependence dielectrophoresis technique for bridging graphene nanoribbons", The 81th autumn meeting of Japan Society of Applied Physics (JSAP) 2020, Online Virtual Meeting.

POSTER PRESENTATION

1. **Wahyu Waskito Aji**, Hirofumi Tanaka.," Study of Trapping Condition on Dielectrophoresis to Fabricate GNRs Devices", International Symposium on Applied Engineering and Sciences (SAES) 2018., Kitakyushu – Japan.
2. **Wahyu Waskito Aji**, Hirofumi Tanaka.," Study of Trapping Condition on Dielectrophoresis to Fabricate GNRs Devices", The 66th spring meeting of Japan Society of Applied Physics (JSAP) 2019, Ookayama – Japan.
3. **Wahyu Waskito Aji**, Hirofumi Tanaka.," Study of Trapping Condition on Dielectrophoresis to Fabricate GNRs Devices", 10th Molecular Architectonics Meeting 2019, Kitakyushu – Japan.

ACKNOWLEDEMENT

Thanks to Almighty Allah for everything so that I could finish my Ph.D. study.

Firstly, I would like to express gratitude to my supervisor, Prof. Hirofumi Tanaka for the continuous support during my Ph.D Study and research, for his patient, motivation, enthusiasm, and immense knowledge. His guidance helped me in all the time of research and writing of this dissertation.

Secondly, I would like to thank Ministry of Education, Culture, Sport, Science and Technology (MEXT) of Japan for funding my Ph.D study through Global Assistive Adaptive Robotic (GAAR) Program as well as the lecturers and staffs of Kyushu Institute of Technology for their kind assistance. Special acknowledgment is also extended to the people who help me at/during some experiment: Dr Yuki Usami (Kyushu Institute of Technology), Dr Guarav Kapil (Kyushu Institute of Technology), Semiconductor Center Kitakyushu Science and Research Park (KRSP) and Yamaguchi University for electrode fabrication, Kyushu University for Raman analysis. Also, thanks to all Tanaka Lab's member and Indonesia Student Association of Kitakyushu for help and support during my Ph.D study.

To my wife (Tika Erna Putri), my parents (Tugino, Sutarmi, Sugiyono and Tutik Ernawati), and all big family's member, thank you for the caring, patience, love and endless support.

Wahyu Waskito Aji

September, 2020